KfK 5213
Juli 1993

Aspects of Modelling a Thermal Two-component Plasma and its Approximation with Explicit Numerical Methods

R. Schneider, C.-D. Munz
Institut für Neutronenphysik und Reaktortechnik

Kernforschungszentrum Karlsruhe

KERNFORSCHUNGSZENTRUM KARLSRUHE
Institut für Neutronenphysik und Reaktortechnik

KfK 5213

Aspects of Modelling a Thermal Two-component Plasma and its Approximation with Explicit Numerical Methods

R. Schneider and C.-D. Munz

Kernforschungszentrum Karlsruhe GmbH, Karlsruhe

Als Manuskript gedruckt

Kernforschungszentrum Karlsruhe GmbH
Postfach 3640, 7500 Karlsruhe 1

ISSN 0303-4003

Abstract

In this report, a longitudinal model of a thermal two-component plasma is considered. A compact description to solve numerically the resulting coupled inhomogeneous model system is developed. The numerical techniques applied are based on high resolution shock-capturing schemes for the hydrodynamic part which have been developed for the numerical solution of nonlinear hyperbolic conservation laws, recently. A new explicit numerical method is proposed to calculate the electric field which couples the different plasma components. Here, the comprehensive information available from the flux calculation of the high resolution upwind schemes is used. Furthermore, a new tracking method will be briefly reviewed which plays an important role in handling the problem of a plasma expanding into a vacuum. Numerical results for three examples are presented which may be considered as proofs of principle for the applicability and efficiency of the explicit numerical methods in plasma simulation.

Aspekte zur Modellierung eines thermischen Zwei-Komponenten Plasmas und seiner Behandlung mit expliziten numerischen Methoden

Überblick

In diesem Bericht wird ein longitudinales Modell eines thermischen Zwei-Flüssigkeitsplasmas betrachtet und unter Verwendung numerischer Methoden untersucht. Eine gestraffte Zusammenfassung der zugrunde gelegten numerischen Methoden soll eine Vorstellung davon geben, wie das resultierende inhomogene Modellsystem gelöst wurde. Die verwendeten Approximationstechniken sind als "high resolution shock-capturing " Schemata bekannt und wurden zur numerischen Lösung von nichtlinearen Erhaltungsgleichungen entwickelt. Desweiteren wird eine Methode dargelegt, wie das elektrische Feld, welches die verschiedenen Plasmakomponenten koppelt, auf explizitem Wege aus der vorhandenen Information der Flußberechnung gewonnen werden kann. Um das Problem der Plasmaexpansion ins Vakuum sauber behandeln zu können, wird weiterhin eine neue, vor kurzem vorgeschlagene Tracking-Methode beschrieben und angewandt. Numerische Resultate, die wir anhand dreier Testbeispiele erhielten, überzeugen uns von der Verwendbarkeit und Effizienz der expliziten Methoden im Bereich der Plasmasimulation.

Contents

I. Introduction

Providing high power densities in matter necessary for inertial confinement fusion, is a challenging problem for pure science as well as for technology. With respect to this basic research problem, great progress in generating high-power ion beams have been made during the last two decades [1]. For this purpose the pulsed power line KALIF [2] is available at the Nuclear Research Center in Karlsruhe (KfK). Optional, the high power KALIF puls can be feeded into different ion diodes, developed at the KfK [3, 4, 5], where it is converted into an intense ion beam. Modern plasma generation techniques provide an excellent tool to produce a uniform plasma layer in front of the ion diode electrodes, yielding an ion beam power of approximately 1 TW [5]. In order to increase this ion beam power with further facilities like the KALIF-HELIA extension, it is necessary to reduce the observed microscopic divergence. The origin of this divergence is traced back to diode effects [5] like instabilities, occuring in the electrode plasmas or/and in the dilute plasma region inside the diode gap. Therefore, of first priority should be the understanding of the mechanisms leading to the observed microscopic divergence.

To get a deeper insight into the fundamental physical phenomena occuring inside the ion diodes, and hence, a better interpretation of the experimental results, extensive numerical simulations have been performed. For that purpose the two-dimensional time-independent particle-in-cell code BFCPIC is used, which is an extension of the usual PIC-codes to boundary-fitted coordinates [6, 7]. Although, this code is an excellent tool for the optimization of the design of technical relevant diodes [8] and the resulting focussing properties, there remains an inconsistency between the measured and predicted ion current densities [5]. This discrepancy may be attributed to the fact that in BFCPIC several physical phenomena are disregarded.

One challenging problem in this context is the adequate temporal modelling of the neutral plasmas in the vicinity of the cathode and anode. These plasma layers, covering the emitting electrodes, appear in an approximately spontaneous manner after the ion source is switched on. Little is known about the behavior of these plasma layers, which are in principle the input boundary values for BFCPIC-calculations. In this paper we propose a model for the mathematical description of the temporal evolution of plasma layers and develop a numerical method for these equations.

This paper is organized as follows. In chapter II we list the equations of the considered longitudinal model of a thermal two-component plasma. This model should be appropriate to give insight into the complex behavior of the plasma layers in front of the emitting electrodes of the ion diodes. Subsequently, in chapter III we describe the

numerical techniques applied, necessary for the investigation of the plasma model in mind. Our approach is based on the so-called Godunov-type methods, which are are explicit schemes in conservation form. Within these schemes the approximation of the fluxes between adjacent grid zones are determined by solving Riemann problems approximately. Using the information obtained by the flux calculation we receive an explicit numerical scheme to calculate the electric field, which is originally determined by the Poisson equation. This is a new approach in this context. The limit when one of the initial states of the general Riemann problem tends to vacuum is called the "vacuum Riemann problem". Its solution is used for the construction of a tracking method for a plasma vacuum boundary, proposed by Munz, recently [9]. This tracking method plays an important role, if we consider the problem of a plasma expanding into a vacuum, underlying an Eulerian frame of reference as the computational domain. In chapter IV we present some results for three test problems which show the quality and the properties of the methods applied. Finally, in chapter V we give a brief summary of the results and a short outlook of the activities planned in future.

II. Basic Macroscopic Equations of a Thermal Two-Component Plasma

The most general description of a plasma is based on the well known principles of statistical mechanics. Broadly spoken, this means that one is interested in the temporal evolution of the distribution function $f_\alpha(\mathbf{x},\mathbf{v},t)$ in the phase space for each plasma component α (α = electrons,ions). It is a well known fact that the resulting equation posses a non-closed character which reflects the hierachy problem being an inherent difficulty in statistical mechanics (see e.g. [10]). Applying approximation methods, for example the weak coupling approximation, and omitting binary collisions of the particles, leads finally to the non-linear Vlasov equation. This collisionless kinetic equation, coupled to the full set of Maxwell equations form a basic system of equations which is a comprehensive mathematical model for many problems in plasma physics. Because in this paper we are interested in the the macroscopic description rather than in the microscopic description of a plasma, we have to calculate the moments of the local distribution function f_α. This means, that the local densities of interest $Q_\alpha(\mathbf{x},t)$ are expressed as averages in velocity space evaluated with the distribution function f_α:

$$Q_\alpha(\mathbf{x},t) =< Q(\mathbf{v}) >= \frac{1}{n_\alpha(\mathbf{x},t)} \int d\mathbf{v} Q(\mathbf{v}) f_\alpha(\mathbf{x},\mathbf{v},t) \qquad (2.1a)$$

where the number density $n_\alpha(\mathbf{x},t)$ of the species α (=electrons,ions) is given by

$$n_\alpha(\mathbf{x},t) = \int d\mathbf{v} f_\alpha(\mathbf{x},\mathbf{v},t). \qquad (2.1b)$$

For a detailed discussion in defining the local densities as well as evaluating the moments of the local distribution function f_α we refer to the literature [10 – 13]. Starting from the Vlasov equation and using the definitions (2.1), we finally obtain the macroscopic equations of a thermal plasma ([10 – 14])

$$\partial_t n_\alpha + \partial_j \left(n_\alpha v_{\alpha j} \right) = 0 \qquad (2.2a)$$

$$\partial_t \left(n_\alpha v_{\alpha i} \right) + \partial_j \left[n_\alpha v_{\alpha i} v_{\alpha j} + \frac{1}{m_\alpha} \left(p_\alpha \delta^{ij} + \Pi_\alpha^{ij} \right) \right] = \frac{q_\alpha}{m_\alpha} n_\alpha \left(\mathcal{E}_i + \epsilon_{ilm} v_{\alpha l} \mathcal{B}_m \right) \qquad (2.2b)$$

$$\partial_t \tilde{e}_\alpha + \partial_j \left[\left(\tilde{e}_\alpha + \frac{p_\alpha}{m_\alpha} \right) v_{\alpha j} + \frac{1}{m_\alpha} \left(h_{\alpha j} + v_{\alpha i} \Pi_\alpha^{ij} \right) \right] = \frac{q_\alpha}{m_\alpha} n_\alpha v_{\alpha j} \mathcal{E}_j, \qquad (2.2c)$$

expressing the conservation of density, momentum, and energy, respectively. Here, q_α and m_α denotes the charge and mass of the species α. The symmetric total pressure tensor $\mathbf{P}_\alpha^{ij}$ is decomposed into the scalar pressure p_α times the unit tensor δ^{ij} and

the traceless tensor Π_α^{ij}. Furtermore, $\mathbf{v}_\alpha$ is the velocity and $\mathbf{h}_\alpha$ stands for the heat flux vector of the particles of species α. The total energy density $\tilde{e}_\alpha$ is given by

$$\tilde{e}_\alpha = \frac{1}{2} n_\alpha \mathbf{v}_\alpha^2 + \frac{n_\alpha \epsilon_\alpha}{m_\alpha} \tag{2.2d}$$

where ϵ_α denotes the internal energy. The electric and magnetic field, denoted here as $\mathcal{E}$ and $\mathcal{B}$, are obtained by the full set of Maxwell equations. In the usual SI-unit system it is given by

$$\epsilon_{ijk} \partial_j \mathcal{B}_k = \frac{1}{c^2} \partial_t \mathcal{E}_i + \mu_0 J_i, \tag{2.3a}$$

$$\epsilon_{ijk} \partial_j \mathcal{E}_k = -\partial_t \mathcal{B}_i, \tag{2.3b}$$

$$\partial_j \mathcal{E}_j = \frac{\rho}{\epsilon_0}, \tag{2.3c}$$

$$\partial_j \mathcal{B}_j = 0. \tag{2.3d}$$

For the equations of a thermal plasma (2.2) as well as for the Maxwell equations we make use of the usual sum convention, which means, that we sum over all latin indices appearing doubly. The symbol ϵ_{ijk} stands for the total antisymmetric tensor. Furthermore, we use the obvious abbreviations $\partial_t = \frac{\partial}{\partial t}$ and $\partial_j = \frac{\partial}{\partial x_j}$.
The charge density ρ and the electric current density $\mathbf{J}$, known as the source terms of the Maxwell equations, are obtained from

$$\rho = \sum_\alpha q_\alpha n_\alpha, \tag{2.3e}$$

$$\mathbf{J} = \sum_\alpha q_\alpha n_\alpha \mathbf{v}_\alpha. \tag{2.3f}$$

Because we have to sum over all α in equation (2.3e) and (2.3f), the Maxwell equations couple the different components of the thermal plasma, described by (2.2).
For sake of simplicity, we suppose that the local distribution function $f_\alpha(\mathbf{x}, \mathbf{v}, t)$ of the different species α is close to a Maxwellian. Therefore, the heat flux $\mathbf{h}_\alpha$ and the traceless pressure tensor Π_α will be neglected in the following considerations. Obviously, the equations of the thermal plasma (2.2) and the Maxwell equations (2.3) do not form a closed system. To overcome this incompletess, we have to specify an equation of state

$$p_\alpha = p_\alpha(n_\alpha, \epsilon_\alpha), \tag{2.4}$$

which relates the pressure to the density and the internal energy.
The equations (2.2) to (2.4) set up the general macroscopic model of a thermal two-componet plasma which should be the starting point in getting a simpler model, called in the following **the longitudinal model of a thermal two-component**

plasma.

The physical situation in mind can be summarized in the following manner. We consider a plasma for which the plasma parameter N_p ($= \frac{4\pi}{3}\lambda_D^3 n_0, \lambda_D$ is the Debye length, n_0 is the characteristic density) is very large compared to one (weak coupling). This means, that the importance of the Coulomb interaction is negligible compared to the thermal energy. Obviously, the condition $N_p \gg 1$ can be reached in two ways. For a given density, the condition is satisfied for sufficient high temperatures, or alternatively, for a given temperature, it holds for sufficiently low density. Because the ratio of collision frequency between electrons and ions (ν_{ei}) to the plasma frequency (ω_{p0}) is approximately the inverse of the plasma parameter, each component of the plasma lives for a long time in a quasi equilibrium at different temperatures, in general (see e.g. [10]). Consequently, the plasma regarded here will be treated as a mixture of two independent perfect gases.

For the further considerations, we restrict ourselves to one dimension in space (x coordinate). Additional, the magnetic field $\mathcal{B}$ should be zero, and from the remaining vector quantities occuring in (2.2) we consider only the x component. With regard to the numerical methods, discussed in the next chapter, we rewrite the equations (2.2) for our purpose into the compact conservation form [15]:

$$\partial_t \mathbf{u}_\alpha + \partial_x \mathbf{f}(\mathbf{u}_\alpha) = \mathbf{q}(\mathbf{u}_\alpha). \tag{2.5a}$$

Here, $\mathbf{u}_\alpha$ denotes the vector of the conserved variables of each plasma component α, and is given by

$$\mathbf{u}_\alpha = \left(N_\alpha, \mathcal{M}_\alpha, e_\alpha\right)^T, \tag{2.5b}$$

where the calligraphic $\mathcal{M}$ stands for the momentum $\mathcal{M}_\alpha = N_\alpha V_{\alpha x}$. The vector functions $\mathbf{f}(\mathbf{u}_\alpha)$ and $\mathbf{q}(\mathbf{u}_\alpha)$, usually called the Euler flux in in x direction and the vector of the source terms, respectively, are defined as

$$\mathbf{f}(\mathbf{u}_\alpha) = \left(N_\alpha V_{\alpha x}, N_\alpha V_{\alpha x}^2 + \frac{\Pi_\alpha}{M_\alpha}, N_\alpha V_{\alpha x} H_\alpha\right)^T, \tag{2.5c}$$

$$\mathbf{q}(\mathbf{u}_\alpha) = \left(0, S_\alpha N_\alpha E_x, S_\alpha N_\alpha V_{\alpha x} E_x\right)^T. \tag{2.5d}$$

In the longitudinal case considered, the equation which couple the two plasma components is given by the Poisson equation

$$\partial_x E_x = \sum_\alpha S_\alpha M_\alpha N_\alpha, \tag{2.6}$$

only where S_α is the abbreviation for the expression $\Omega_p \frac{Q_\alpha}{M_\alpha}$.

Because of the general nature of the problems, considered here, dimensionless quantities

are introduced in the model equations (2.5) and (2.6). The characteristic length of the problem is λ_0. The dimensionless velocity in x direction $V_{\alpha x}$, particle mass M_α, and particle charge Q_α are obtained from the corresponding quantities in (2.2) by normalizing them to v_0, m_0 and e_0, respectively. The time is measured in units of $t_0 = \lambda_0/v_0$. Furthermore, with the characteristic density n_0 and temperature T_0 and combinations of these two quantities ($p_0 = n_0 T_0$; $E_0 = \sqrt{\frac{n_0 T_0}{\epsilon_0}}$, ϵ_0 electric permittivity of vacuum), the dimensionless density N_α, the pressure Π_α, and electric field in x direction E_x are easily defined. The dimensionless plasma frequency $\Omega_p = \omega_{p0} t_0 = \frac{\lambda_0}{\lambda_D}$ ($\omega_{p0}^2 = \frac{e^2 n_0}{\epsilon_0 m_0}$) is a measure of space charge effects.
For a perfect gas the equation of state has the simple form

$$\Pi_\alpha = \frac{2}{f} N_\alpha \in_\alpha \tag{2.7a}$$

where $\in_\alpha$ is the dimensionless internal energy. The degree of freedom f of a perfect gas is related to the ratio of specific heat capacities via $\gamma = \frac{f+2}{f}$. Then we find for the dimensionless total energy e_α and the enthalpy H_α the following expressions

$$e_\alpha = \frac{1}{2} N_\alpha V_{\alpha x}^2 + \frac{f}{2} \frac{\Pi_\alpha}{M_\alpha}, \tag{2.7b}$$

$$H_\alpha = \frac{1}{N_\alpha}\left(e_\alpha + \frac{\Pi_\alpha}{M_\alpha}\right) = \frac{1}{2} V_{\alpha x}^2 + \frac{f}{2} C_{s\alpha}^2, \tag{2.7c}$$

respectively, where $C_{s\alpha}$ denotes the dimensionless velocity of sound, defined as

$$C_{s\alpha} = \sqrt{\frac{1}{M_\alpha} \frac{\partial \Pi_\alpha}{\partial N_\alpha}}. \tag{2.7d}$$

The equations (2.5), (2.6) and (2.7) set up the one dimensional mathematical model of a thermal two-component plasma where collisions are excluded. This simple model cannot be solved analytically in general. Therefore, we need appropriate methods for calculating the numerical solution of the model equations (2.5)-(2.7) to get a comprehensive insight into the complex behavior of a thermal neutral plasma.

III. Numerical Framework

In this chapter we shall be concerned with the methods for solving the longitudinal model of a thermal two-component plasma (2.5), (2.6) numerically. Therefore, we consider in the first section briefly the numerical techniques applied for treating the nonlinear inhomogeneous system of conservation laws (2.5a). Afterwards, we introduce an explicit numerical approach for solving a modified Poisson equation which corresponds to (2.6). Some general remarks of treating numerically the problem of a plasma expanding into a real vacuum will be presented in the next section.

A. Numerical solution of the inhomogeneous conservation system

Among the various methods proposed in the literature to solve numerically the system of nonlinear conservation laws (2.5a), the so-called high resolution shock-capturing schemes are chosen, which have been developed recently (see e.g. [16]). Especially, these methods are developed for the numerical solution of nonlinear hyperbolic conservation laws and, furthermore, play an important role in compressible hydrodynamics.
Constructing those numerical schemes, the information of the local wave propagation structure of the problem is obtained by solving the Riemann problem (RP). The RP is the initial value problem for the homogeneous conservation laws (2.5a) (neglecting here the rhs of (2.5a)) with piecewise constant initial data having a single discontinuity at $x = 0$

$$\mathbf{u}(x,0) = \begin{cases} \mathbf{u}_l, & x < 0 \\ \mathbf{u}_r, & x > 0 \end{cases} . \tag{3.1}$$

The key problem in developing efficient numerical methods based on the RP, is to find a good approximate solution of the RP.
The idea of an approximation scheme for the nonlinear conservation laws using the RP solution is due to Godunov [17]. He supposed that the approximate solution at a time $t = t_n$ is constant within a grid cell (see figure 3.1). To elude an interaction between the solutions of the local RP, occuring at each grid zone interface, he further suppose that

$$\frac{\Delta t}{\Delta x} |a_{max}| \leq \frac{1}{2}$$

holds, where a_{max} denotes the maximum velocity of the propagating waves. Afterwards, Godunov determined the exact solution of the RP at each grid zone interface, having the form

$$v = v\left(\frac{x - x_{i+1/2}}{t - t_n}; \mathbf{u}_i^n, \mathbf{u}_{i+1}^n \right),$$

and averaged these solutions over the interval $I_i = [x_i, x_{i+1}]$ in oder to get a piecewise constant approximate solution at time $t = t_{n+1}$. Often, it is troublesome or even impossible to get an exact solution of the RP. And obviously, because of the final averaging process in the Godunov scheme, only small amount of the entire information provided by the exact solution is used for the further iterations.

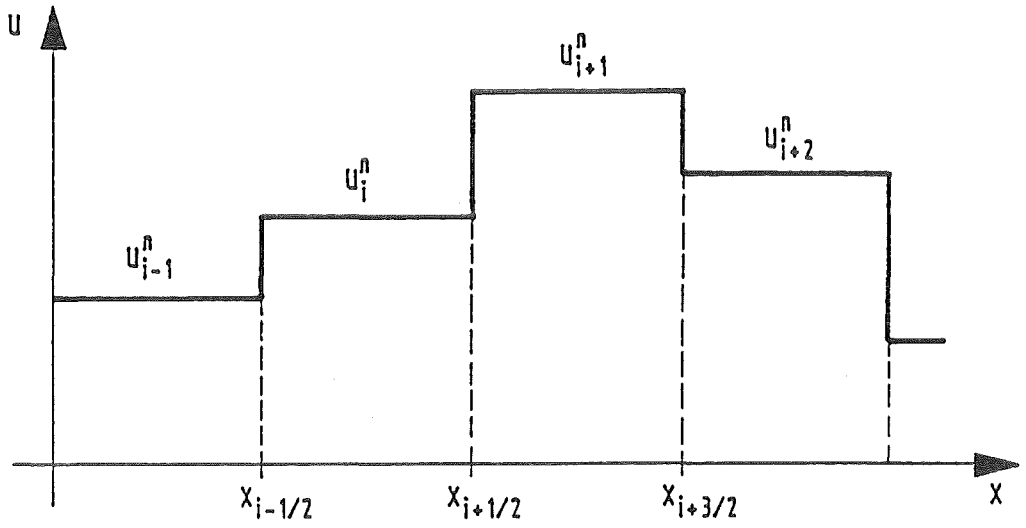

Figure 3.1: Piecewise constant approximate solution

Therefore, we make use of an approximate solution of the RP which has been proposed by Harten, Lax and van Leer (HLL) [18]. The basic idea of the HLL-method is to replace the intermediate states of the general RP by an averaged one (see figure 3.2). The approximate Riemann solution of the HLL-method has the form

$$\mathbf{w}\left(\frac{x}{t}; \mathbf{u}_l, \mathbf{u}_r\right) \begin{cases} \mathbf{u}_l, & \frac{x}{t} < a_l \\ \mathbf{u}_{lr}, & a_l < \frac{x}{t} < a_r \\ \mathbf{u}_r, & \frac{x}{t} > a_r \end{cases}, \tag{3.2}$$

where a_l, a_r denotes the minimum and maximum propagation velocity, respectively. Algorithms where the exact solution of the RP is replaced by an approximate one, are the so-called Godunov-type schemes. It can be shown [16, 19] that Godunov-type

schemes are explicit schemes in conservation form, represented by

$$\mathbf{u}_{\alpha,i}^{n+1} = \mathbf{u}_{\alpha,i}^{n} - \lambda\left(\mathbf{g}_{\alpha,i+1/2}^{n} - \mathbf{g}_{\alpha,i-1/2}^{n}\right), \qquad \lambda = \frac{\Delta t}{\Delta x}. \tag{3.3}$$

Here, $\mathbf{g}_\alpha = \mathbf{g}_\alpha(\mathbf{u}_l, \mathbf{u}_r)$ denotes the numerical flux, which is determined by the approximate RP solution and is an appropriate approximation of the Euler flux $\mathbf{f}$ given by equation (2.5c).

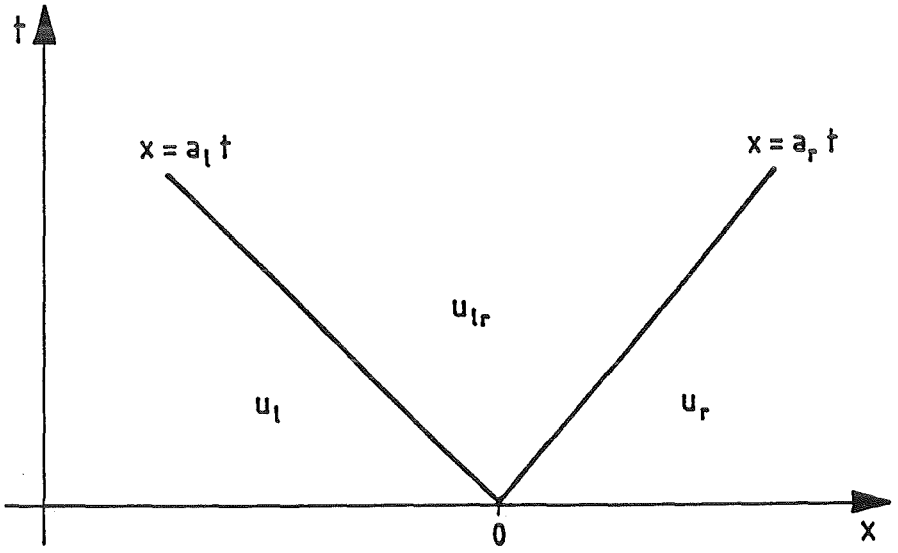

Figure 3.2: Approximate Riemann solver for the HLL-method

Especially, for the HLL-method the numerical flux is obtained form

$$\mathbf{g}_\alpha^{(HLL)}(\mathbf{u}_l, \mathbf{u}_r) = \frac{1}{a_r^+ - a_l^-}\left[a_r^+ \mathbf{f}(\mathbf{u}_l) - a_l^- \mathbf{f}(\mathbf{u}_r) + a_l^- a_r^+ (\mathbf{u}_r - \mathbf{u}_l)\right], \tag{3.4a}$$

where a_l^- and a_r^+ is the abbreviation for

$$a_l^- = \mathrm{MIN}(0, a_l) \qquad a_r^+ = \mathrm{MAX}(0, a_r), \tag{3.4b}$$

respectively.
The approximation techniques, briefly described above are only accurate to the first

order in time. The extension to second order accuracy can be done in a straightforward mannner, applying the MUSCL (Monotonic Upwind Schemes for Conservation Laws) approach proposed by van Leer (see e.g. [20]). A detailed description and discussion of the properties of the second order extension can also be found in [19].
The general advantage of the numerical methods under consideration is twofold. Calculating the numerical flux $\mathbf{g}_\alpha$ between adjacent grid cells during one time step, the direction of nonlinear wave propagation is directly incorporated into the solution scheme. Hence, they sharply resolve discontinuities without generating spurious oscillations. In smooth parts of the flow the approximation is second order accurate in space and time.
Interested finally in the numerical solution of the inhomogeneous system of conservation equations (2.5a), we apply a splitting method described by Marchuk [21]. That means for our purpose, that we have to solve in a first step the homogeneous conservation laws with the methods described above. After this transport step, we consider the influence of the source terms $\mathbf{q}(\mathbf{u}_\alpha)$ (2.5d). Therefore, we have to solve the system of ordinary differential equations

$$\frac{d}{dt}\mathbf{u}_\alpha = \mathbf{q}(\mathbf{u}_\alpha). \tag{3.5}$$

With the initial condition $\mathbf{u}_{\alpha 0}$, provided by the solution of the homogeneous system, the differential equation (3.5) can be solved numerically with standard methods (see e.g. [22]). But before we can evaluate the solution of the last equation, we need the electric field which is determined by equation (2.6). How to solve this equation is the subject of the next section.

B. Modified Poisson equation and its numerical solution with explicit methods

In the longitudinal model of a thermal two-component plasma considered, the Poisson equation (2.6) couples the different components of the plasma. Instead of solving this elliptic equation with the usual methods proposed in literature [23], we want to make use of the comprehensive information available from the explicit numerical schemes described above. Additionally, we should have the possibility to include in further considerations a time-dependent external potential, extending the present model to a more realistic model for the electrodes of the ion diodes.
For that purpose, we first rewrite the explicit conservation scheme (3.3) in the following manner

$$N_{\alpha,i}^{n+1} = N_{\alpha,i}^{n} - \lambda\left(G_{\alpha,i+1/2}^{n} - G_{\alpha,i-1/2}^{n}\right), \qquad \lambda = \frac{\Delta t}{\Delta x}, \tag{3.6}$$

which is the starting point for the further discussion. In the scalar equation (3.6) $N^n_{\alpha,i}$ and $G^n_{\alpha,i+1/2}$ denotes the density and the corresponding numerical flux, respectively. Obviously, (3.6) represent the first column of the vector equation (3.3). Using central finite differences, the Poisson equation (2.6) at the time level $t = t_{n+1}$ is given by

$$E^{n+1}_{i+1} - E^{n+1}_i = \Delta x \sum_\alpha S_\alpha M_\alpha \frac{1}{2}\Big(N^{n+1}_{\alpha,i+1} + N^{n+1}_{\alpha,i}\Big), \tag{3.7}$$

where Δx is the distance of the spatial grid points, which is located equidistantely for sake of simplicity. Inserting (3.6) into (3.7) and assuming that the Poisson equation holds at each time step, we obtain after some manipulations

$$\mathcal{F}^{\Delta t}_{i+1} - \mathcal{F}^{\Delta t}_i = 0 \tag{3.8a}$$

where $\mathcal{F}$ is given by the expression

$$\mathcal{F}^{\Delta t}_i = E^{n+1}_i - E^n_i + \Delta x \sum_\alpha S_\alpha M_\alpha \frac{\lambda}{2}\Big(G^n_{\alpha,i+1/2} + G^n_{\alpha,i-1/2}\Big). \tag{3.8b}$$

Because equation (3.8a) represents a perfect finite difference in space, the electric field is given by (3.8b) except for a constant C^n which may be time-dependent, but independent of position. Adding this constant, the electric field at the time level $t = t_{n+1}$ has the form

$$E^{n+1}_i = E^n_i - \Delta t \Lambda^n_i + C^n \tag{3.9a}$$

where the current density Λ^n_i, obtained from the relation

$$\Lambda^n_i = \sum_\alpha S_\alpha M_\alpha \frac{1}{2}\Big(G^n_{\alpha,i+1/2} + G^n_{\alpha,i-1/2}\Big), \tag{3.9b}$$

is expressed as an average of the numerical fluxes $G^n_{\alpha,i+1/2}$ and $G^n_{\alpha,i-1/2}$. Using these fluxes which actually advance the density $N_{\alpha,i}$ in time (see equation (3.6)), guarantee that the charge will be conserved. This means, that an integral form of the Poisson equation is satisfied, and equation (3.9a), having the appearance of Ampère's law, is an appropriate numerical approximation for calculating the electric field, originally determined by equation (2.6).

In the following, we want to outline a way how to determine the, in general, time-dependent constant C^n. Obviously, the necessary condition ($\epsilon_{ijk}\partial_j E_k = 0$) for expressing the electric field as a gradient of a potential ϕ is fulfilled in our model, resulting in the equation

$$-\frac{d\phi(x,t)}{dx} = E(x,t). \tag{3.10a}$$

Integrating the last equation over the intervall $[0, L]$, we obtain

$$-V(t) = -\left[\phi(L,t) - \phi(0,t)\right] = \int_0^L dx E(x,t), \tag{3.10b}$$

where $V(t)$ denotes the time-dependent external voltage. Approximating the integration in (3.10b) numerically by the extended trapezoidal rule (see e.g. [24])

$$\int_0^L dx f(x) \approx \frac{\Delta x}{2}\left[f(x_{1/2}) + f(x_{N+1/2})\right] + \Delta x \sum_{k=1}^{N-1} f(x_{k+1/2}) := \Delta x \sum_k^{\dagger} f_{k+1/2},$$

the corresponding discretized version of (3.10b) reads as

$$-V^n = -\left[\phi^n_{N+1/2} - \phi^n_{1/2}\right] = \Delta x \sum_k^{\dagger} E^n_{k+1/2} \tag{3.10c}$$

where we used the symbolic abbreviated notation $\Delta x \sum_k^{\dagger}$ for the integration. To obtain now an equation for the unknown constant C^n we multiply equation (3.9a) by $-\Delta x$ and sum over k from 1 to N. Making furthermore explict use of equation (3.10c) we find finally for C^n the expression

$$C^n = -\frac{1}{L}\left(V^{n+1} - V^n\right) + \frac{\Delta t}{L}\Delta x \sum_k^{\dagger} \Lambda^n_{k+1/2}. \tag{3.11}$$

After the excursion in computing the position independent but time-dependent constant C^n, we are able to calculate the electric field E_i^{n+1} at the new time level $t = t_{n+1}$. For that purpose we only refer to quantities available at the time level $t = t_n$ with exception of the external potential, which should cause no difficulties because the temporal step size Δt is always known.
A remaining problem in solving equation (3.9) is to specify the boundary values. However, this problem could be resolved in a simple manner, if we consider for example periodic boundary conditions for the density $N^n_{\alpha,i}$ which reads as

$$N^n_{\alpha,0} = N^n_{\alpha,N}$$

$$N^n_{\alpha,N+1} = N^n_{\alpha,1},$$

and are true for all times t. The applicability of equation (3.9) will be demonstrated in the next chapter where we will consider well known problems without an external circuit ($C^n = 0$) as examples.

With regard to further applications of the proposed explicit electric field solver (3.9), especially in the field of ion diode physics, we close this section with a remark which

may be helpfull for investigations in the near future. Inserting (3.11) into equation (3.9a) and carry out some rearrangements, we obtain the so-called Ampère-type equation in the discrete form

$$\frac{1}{\Delta t}\left(E_i^{n+1} - E_i^n\right) + \Lambda_i^n = -\frac{1}{L}\frac{1}{\Delta t}\left(V^{n+1} - V^n\right) + \frac{1}{L}\Delta x \sum\nolimits_k^{\dagger} \Lambda_{k+1/2}^n \qquad (3.12)$$

which plays an important role in the context of the current-voltage relation in a time-dependent diode [25] . Equation (3.12) states that the total current density (lhs of (3.12)) in a diode is not only given by the temporal changing of the external voltage but, additionally, by the line-integrated current.

C. Review of the tracking method for the plasma flow into vacuum

Preliminary, to motivate the subject of the following discussion, we will introduce a physical example which should be kept in mind for the further considerations. Therefore, we suppose that a plasma layer is generated in front of the electrode A of a diode. The electrode is situated at the left side of the computational domain and the initial plasma profile has an extension up to $x = x_0$. For positions larger than x_0 there should be vacuum. This idealized situation may be characterized in the conserved variables as

$$\left(N_\alpha, N_\alpha V_{\alpha x}, e_\alpha\right) = \begin{cases} (1, 0, \frac{f}{2}) & \text{for} \quad x < x_0 \\ (0, 0, 0) & \text{for} \quad x > x_0 \end{cases}, \qquad (3.13)$$

which is obvious very similar to (3.1). The special additional assumptions made in (3.13) consists in the fact that the initial velocity for $x < x_0$ is zero and the pressure is equal to one. Interested now in the temporal evolution of the initial data (3.13), we have to solve in general the model system (2.5), (2.6) with the numerical methods descriebed in section III.A and III.B. To simplify the problem for the moment, we restrict ourselve to a simpler model, namely, we assume that the electric field vanishes and thus we are left with the homogeneous conservation laws described by (2.5a) neglecting the rhs of (2.5a). Obviously, the situation under consideration corresponds to a single-fluid plasma, expanding into vaccum.
The arising numerical problems for this example are the same as for the expansion of a gas flow into vaccum. In the context of gas dynamics it is usual to apply the numerical methods mentioned in section A (see e.g. [16, 19])to solve the Euler equations, which are equivalent to the homogeneous equation (2.5a).

The main problem in solving numerically the Euler equations with the initial data (3.13) can be summarized in the following manner. If the homogeneous conservation laws (2.5a) are formulated in an Eulerian frame of reference, which is fixed in space, the computational domain contains the plasma region, a plasma vacuum boundary and a vacuum region. Because the Euler equations are based on the continuum assumption (which means that f_α is a smooth function in x, see chapter I), they are no longer valid in the vacuum and a numerical approximation of these equations will fail. That means the problem (2.5a) with initial data (3.13) is not a real initial value problem. It is a free boundary value problem and its numerical solution becomes very complicated. A common procedure is to replace the vacuum region by a plasma of low density and pressure, assuming that the flow into this quasi vacuum is quite similar to the flow into real vacuum and to solve the problem as initial value problem. Since the densities of the quasi vacuum are very low, the numerical method still produces severe difficulties. This is due to the fact that near the plasma vacuum interface the dominant energy mode becomes kinetic. Usually, as it is pointed out in section III.A, the numerical approximation of the homogeneous conservation laws is performed in the conserved variables density, momentum and total energy (see (2.5b)). To obtain the internal energy, which is the key quantity for computing pressure and temperature, we subtract the kinetic energy from the total energy. In low density regions any small rounding or truncation error may result in negative internal energy and, consequently, the numerical approximation breaks down. Replacing simply a negativ internal energy value by a small positive one, violates the conservation laws and may generate nonlinear instabilities. Recently, a sophisticated method which avoids the difficulties mentioned above, was proposed by Munz [9]. The essential feature of this tracking method is that the plasma vacuum interface in the Eulerian frame of reference is monitored in time. Several aspects of this method, necessary to assess the results presented in chapter IV, should be outlined in the following.

An important initial-value problem for the Euler equations (eq.(2.5a) without the rhs) is the Riemann problem with piecewise constant initial data as defined in (3.1). The general solution is given by a fixed point problem, and consists of four constant states $\mathbf{u}_l$, $\mathbf{u}_1$, $\mathbf{u}_2$ and $\mathbf{u}_r$ (see figure 3.3), separated by elementary waves (see e.g. [26]). For our purpose, we suppose that the right state is a shock wave (all variables jump according the Rankine-Hugonoit condition) and the left state represents a rarefaction wave (a continuous transition from the left to the right values). The intermediate states $\mathbf{u}_1$, $\mathbf{u}_2$ are separated by a contact discontinuity, where the density is discontinuous, while the pressure and velocity is constant. From now, we want to consider the situation where the right state $\mathbf{u}_r$ coincide with the vacuum.

The homogeneous conservation equations (2.5a) together with the initial data specified by (3.13) form the so-called "vacuum Riemann problem" (VRP) [9]. As outlined above the VRP is no initial-value problem. It is a free boundary problem, because vacuum is no solution of the Euler equations. But the solution of the VRP may be obtained as a limit of the solution of the usual Riemann problem. The general structure of the solution of the VRP can be understood if we compare figure 3.3 with 3.4.

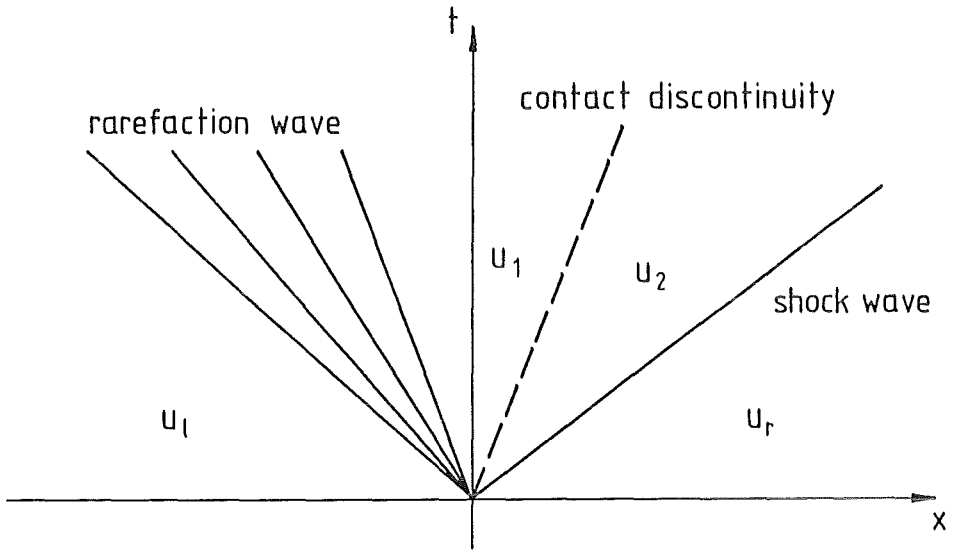

Figure 3.3: Solution of a Riemann problem in (x,t)-diagram

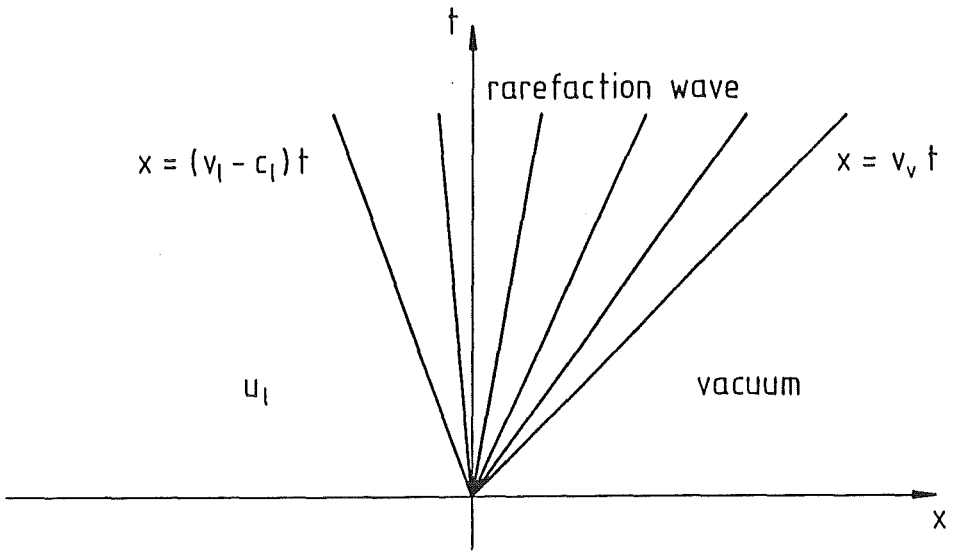

Figure 3.4: Solution of a vacuum Riemann problem in (x,t)-diagram

The contact discontinuity, travelling with the local fluid velocity, set up the interface between plasma and vacuum. Hence, the right state in figure 3.3 disappears. Because the pressure has to be constant across the contact (namely zero), the contact discontinuity also disappears in the sense that it coincides with the right boundary of the left wave. Consequently, the left state is connected to the vacuum by only one elementary wave. Since the Rankine-Hugonoit condition cannot be satisfied in this case, the elementary wave has to be a rarefaction wave. This solution of the VRP can be calculated analytically and is given in appendix A.

In the following considerations we briefly sketch out the numerical framework necessary to overcome the serious problems connected with the plasma vacuum boundary inside the computational domain. Therefore, we assume that the appropriate numerical method to solve the Euler equations is given by (3.3). Using the ideas of Munz [9], we track numerically the plasma vacuum boundary in a first step to get an estimation of the real movement of this interface. Using this information we determine in a second step the numerical flux in the related plasma vacuum grid zone in such a way that the plasma vacuum interface remains sharp.
We assume that the location of plasma vacuum boundary (X_v^n) at the time level t_n is situated in the i-th grid zone (see figure 3.5). The location of the plasma vacuum interface at the time level t_{n+1} is obtained by solving the VRP. According appendix A (omiting here the particle index α) the location of the interface is given by

$$X_v^{n+1} = X_v^n + \Delta t V_v^n \tag{3.14a}$$

with

$$V_v^n = V_l + \frac{2}{\gamma - 1} C_l. \tag{3.14b}$$

The left state $\mathbf{u}_l$ required may be obtained by the formular

$$\mathbf{u}_l = \alpha < \mathbf{u}_i^n > +(1-\alpha)\mathbf{u}_{i-1}^n \tag{3.15a}$$

$$\alpha = \frac{1}{\Delta x}\left(X_v^n - x_{i-1/2}\right), \tag{3.15b}$$

where the knowledge of the location of the plasma vacuum boundary at the time level t_n is used, explicitly. The calculation of the left state $\mathbf{u}_l$ as proposed by (3.15), can be understood in the following way. Since we only use $\mathbf{u}_i^n$ as the left state, waves generated at $x_{i-1/2}$ will interact with the VRP and can change its solution. To guarantee, that these waves do not reach the plasma vacuum interface a constant left state (3.15), must be introduced which is constant within an intervall length of Δx . Because the i-th grid intervall $[x_{i-1/2}, x_{i+1/2}]$ contains plasma as well as vacuum, we ought to

use the over the intervall $[x_{i-1/2}, X_v^n]$ redistributed integral value $< \mathbf{u}_i^n >$ instead of $\mathbf{u}_i^n$:

$$< \mathbf{u}_i^n >= \frac{1}{\alpha}\mathbf{u}_i^n = \left(\bar{N}_i^n, \bar{\mathcal{M}}_i^n, \bar{e}_i^n\right)^T. \qquad (3.16a)$$

We use here the known location of the plasma vacuum boundary. It seems to be favorable to calculate the right hand side of (3.15a) not in the conserved but in the primitive variables N, V and Π. The vector $< \mathbf{w}_i^n >$ in the primitive variables, corresponding to (3.16a) reads as

$$< \mathbf{w}_i^n >= \left(\bar{N}_i^n, V_i^n, \bar{\Pi}_i^n\right)^T, \qquad (3.16b)$$

where we have to emphasize that the velocity is not obtained by its redistributed integral value. Performing the calculation in the primitive variables ensures that Π_l is a convex average of $\bar{\Pi}_i^n$ and Π_{i-1}^n and remains positive. Otherwise, the pressure Π_l has to recalculated from the average of the conservative variables, which may lead in low density regions to the numerical difficulties mentioned already above.

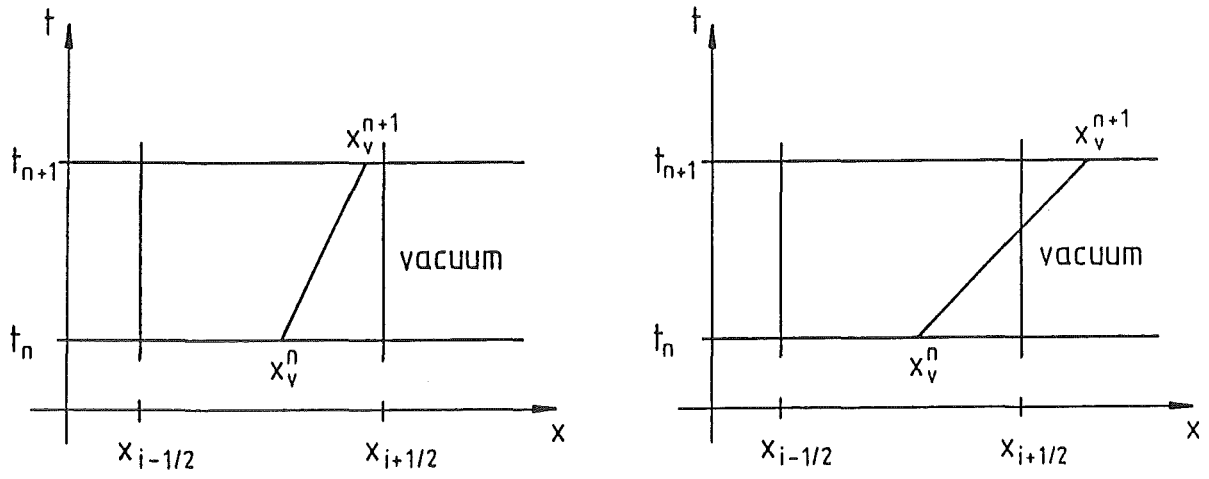

Figure 3.5: Tracking of plasma vacuum boundary within the Eulerian grid

Using the information of the tracking step (3.14) - (3.16) an approximation of the plasma vacuum boundary at the time level t_{n+1} is obtained. The second step make full use of this information to calculate the numerical flux near the plasma vacuum interface. Two different cases are to distinguish which are shown in figure 3.5.

According the left picture in figure 3.5, the grid zone interface at $x = x_{i+1/2}$ belongs to vacuum during the whole time step Δt. Hence, the numerical flux must be zero. What we call case 1 can be summarized as:
If

$$X_v^{n+1} \leq x_{i+1/2}$$

then

$$\mathbf{g}_{i+1/2} = 0. \tag{3.17}$$

The second case becomes evident from the right picture of figure 3.5. Here, the plasma vacuum boundary moves across the grid zone interface during the time step Δt. Clearly, the flux vector at $x_{i+1/2}$ for this cases becomes non zero. A good numerical flux calculation should be obtained by using the fluxes of the exact VRP (see appendix B). Incorporating the information of the tracking step, these fluxes should be taken at $\delta y = x_{i+1/2} - X_v^n$, and averaged over the time step, afterwards. Suppose that the plasma vacuum boundary intersect the vertical line $x = x_{i+1/2}$ at

$$\delta t_n^* = \frac{\delta y}{V_v^n}, \tag{3.18a}$$

Then the intersection of the left rarefaction fan boundary curve with $x = x_{i+1/2}$ is given by

$$\delta t_{n+1}^* = \mathrm{Min}\Big(\Delta t, \frac{\delta y}{V_l - C_l}\Big), \tag{3.18b}$$

where we assume that $V_l - C_l$ is always positive. If $V_l - C_l$ is negative, δt_{n+1}^* should be equal to Δt. Now we are able to résumé case 2 in the compact form:
If

$$X_v^{n+1} > x_{i+1/2}$$

then

$$\mathbf{g}_{i+1/2} = \frac{1}{\Delta t} \int_{\delta t_n^*}^{\delta t_{n+1}^*} dt \mathbf{f}\left[\mathbf{u}(\delta y, t)\right] + \frac{1}{\Delta t}\Big(\Delta t - \delta t_{n+1}^*\Big)\mathbf{f}(\mathbf{u}_l), \tag{3.19}$$

where $\mathbf{u}(\delta y, t)$ is the exact solution of the VRP (see appendix A). The integrals (3.19) can be determined analytically. This is shown in appendix B.
As it will be demonstrated in the next chapter, the numerical scheme (3.14) - (3.19) seems to be suitable to handle the serious problem of a plasma vacuum interface within an Eulerian frame of reference.

Closing this section, we want to make two further remarks. First, instead of calculating the integrals occuring in (3.19), Munz proposed in [9] an extension of the HLL-method to calculate the flux $\mathbf{g}_{i+1/2}$ which substantial reduce the computational effort. Secondly,

he could further show that the numerical scheme (3.14) - (3.19) do not decrease the entropy. This is an important result, which ensures us that the proposed numerical method do not produce unphysical solutions at the vacuum transition.

IV. Test problems and numerical results

A. The finite electron temperature model

In this section we will demonstrate that the calculation of the electric field according the method proposed in III.B is a quite good approximation. Therefore, we consider the finite electron temperature (FET) model which is well-known in the field of plasma physics (see e.g. [27] and references therein). Starting from the longitudinal model of a thermal plasma (2.5), (2.6) the basic equations of the FET model are obtained in a simple manner.
Because the ion mass is much larger compared to the electron mass, the ions should form a fixed, uniform background for the electron fluid. Without loss of generality, we assume that

$$N_i(x,t) = 1$$

$$V_{ix}(x,t) = 0 \qquad (4.1a)$$

for all times. Assuming that the perfect electron gas posses only one degree of freedom ($f = 1, \gamma = 3$), the motion of the electron fluid is finally given by the dimensionless model equations ($M_e = 1$)

$$\frac{DN_e}{Dt} = -N_e \partial_x V_{ex}$$

$$\frac{DV_{ex}}{Dt} = -\frac{1}{N_e}\partial_x \Pi_e + \Omega_p E_x$$

$$\frac{DE_x}{Dt} = \Omega_p V_{ex}$$

$$\Pi_e = N_e^3, \qquad (4.1b)$$

where $\frac{D}{Dt}$ denotes the convective derivative. As it is shown in appendix C, the FET model (4.1) can be solved analytically in the small-amplitude limit. The result obtained in this approximation scheme (see (C.8)) should be the reference solution for the following where the parameter ϵ is hold constant with value $2 \cdot 10^{-3}$.

To study the model system (4.1) numerically we apply the approximation methods briefly reviewed in III.A and III.B. A second order extension of the explicit scheme in conservation form (3.3) according van Leer [20] is used. Thereby, the time step size Δt is controlled in an adaptiv manner via the CFL-condition. The numerical flux $g^n_{\alpha,i+1/2}$ is calculated within the HLL-method and is obtained from (3.4). Because it

is important to have a good estimation of the signal velocities a_l and a_r, we make use of ideas proposed by Roe [28], leading finally to the so-called HLLE-method [19].

Within the extended HLL-method the velocities of the propagating waves are given by

$$\begin{aligned} a_l &= \mathrm{MIN}\big(V_l - C_l, \bar{a}_1\big) \\ a_r &= \mathrm{MAX}\big(V_r + C_r, \bar{a}_3\big), \end{aligned} \tag{4.2a}$$

where we suppressed the particle index α. The quatities $\bar{a}_1$ and $\bar{a}_3$ are obtained by diagonalizing the so-called the Roe matrix (see e.g. [16])

$$\frac{d\mathbf{f}}{d\mathbf{u}}(\bar{\mathbf{u}}) = \mathbf{A}(\bar{\mathbf{u}}) = \mathbf{A}_{lr}$$

with

$$\bar{\mathbf{u}} = \bar{\mathbf{u}}(\mathbf{u}_l, \mathbf{u}_r).$$

Using the flux vector (2.5c) we find for the real eigenvalues of the Roe matrix the result

$$\bar{a}_1 = \bar{V} - \bar{C}, \qquad \bar{a}_2 = \bar{V}, \qquad \bar{a}_3 = \bar{V} + \bar{C}. \tag{4.2b}$$

Here, the crosslines indicate the so-called Roe mean values, which can be obtained from the following relations:

$$\begin{aligned} \bar{V} &= \frac{\sqrt{N_l}V_l + \sqrt{N_r}V_r}{\sqrt{N_l} + \sqrt{N_r}} \\ \bar{H} &= \frac{\sqrt{N_l}H_l + \sqrt{N_r}H_r}{\sqrt{N_l} + \sqrt{N_r}} \\ \bar{C}^2 &= \frac{f}{2}\big(\bar{H} - \frac{1}{2}\bar{V}^2\big). \end{aligned} \tag{4.2c}$$

For more details about the interplay of Roe's ideas and the HLL-method we refer to [19] and the references given therein.

The time-dependent electric field, necessary to calculate the source term vector (2.5d) and consequently to solve the equation (3.5), is determined from relation (3.9). Since we assume that the plasma is not driven by an external voltage, the time-dependent constant C^n is set equal to zero.

The initial profiles for the numerical calculation at $t = 0$ are generated according the exact solution of model (4.1) in the small-amplitude limit (see eqs. (C.8) in appendix C) and are indicated as dotted lines in figure 4.1. Furthermore, the results of the numerical calculation (open squares and circles) together with the exact solution (solid lines) are shown in figure 4.1 for different times ($t = \frac{\pi}{4}, \frac{\pi}{2}, \frac{3\pi}{4}, \pi$). We can ascertain that the numerical solution cover the exact one in an excellent manner.

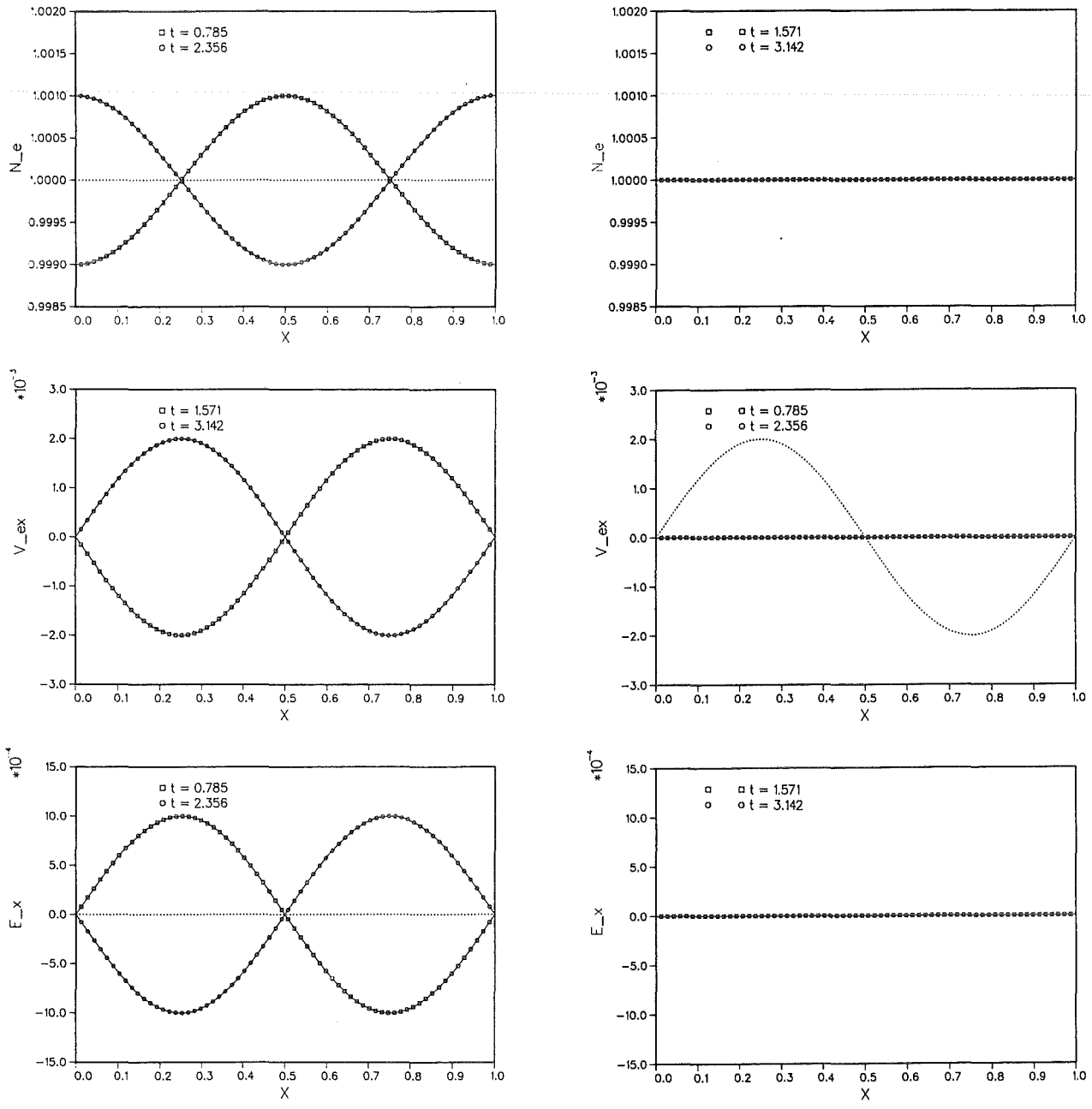

Figure 4.1: Comparison between the exact (solid lines) electron density, electron velocity and electric field and the numerical solution (open squares and circles) for different times.

Especially, we want to emphasize that the electric field $E_x(x,t)$, calculated numerically according (3.9), agree with the exact result in a nearly perfect way. Consequently, we can conclude from figure 4.1 that the method proposed in section III.B to calculate the electric field is a very good and effective approximation. Thereby, we only use the information available from the fluxes $\mathbf{g}^n_{\alpha,i+1/2}$ which actually advance the vector $\mathbf{u}^n_{\alpha,i}$ of the conserved variables in time.

With regard to further applications, especially, to combine a plasma code (like this one used here) with a particle-in-cell code (like BFCPIC) it is necessary to specify the interface between these two codes.
A straightforward method to handle this problem is to solve the ordinary equations of motion

$$\frac{dX_k}{dt} = V_k$$

$$\frac{dV_k}{dt} = A_{FF} \tag{4.4}$$

for a so-called macro particle, accelarated in the flux field of the plasma. The phase space coordinates $\left(X^n_k, V^n_k\right)$ of the k-th macro particle at the time $t = t_n$ should be the appropriate initial values for a subsequent PIC run.

The integration of the Newton equations (4.4) for the k-th macro particle can be carried out numerically in a simple manner. Therefore, we determine in a first step the grid zone where the k-th particle is located at time t_n

$$i_k = \mathrm{INT}\left(\frac{X^n_k - x_0}{\Delta x}\right). \tag{4.5a}$$

Here x_0 denotes the left corner of the equidistant computational domain. Afterwards, we compute the weights associated with the k-th macro particle according

$$w^n_1 = \frac{1}{\Delta x}\left(x_{i_k+1} - X^n_k\right)$$

$$w^n_2 = \frac{1}{\Delta x}\left(X^n_k - x_{i_k}\right). \tag{4.5b}$$

The accelaration A_{FF} of the k-th particle due to the flux field can be calculated, since we know the numerical solution of the FET model (4.1) for the times t_{n-1} and t_n. If it is given, A_{FF} can be calculated from

$$A_{FF} = \frac{1}{\Delta t}\left(\bar{V}^n - \bar{V}^{n-1}\right) \tag{4.5c}$$

with

$$\bar{V}^{n-1} = w^n_1 V^{n-1}_{\alpha,i_k} + w^n_2 V^{n-1}_{\alpha,i_k+1}$$

$$\bar{V}^n = w_1^n V_{\alpha,i_k}^n + w_2^n V_{\alpha,i_k+1}^n.$$

Obviously, the velocity of the macro particle at the new time level t_{n+1} is given by

$$V_k^{n+1} = V_k^n + \Delta t A_{FF}, \tag{4.6a}$$

while the new position can be obtained from

$$X_k^{n+1} = X_k^n + \frac{\Delta t}{2}\left(V_k^{n+1} + V_k^n\right). \tag{4.6b}$$

The dynamical behavior of an ensemble of 900 macro particles is shown in figure 4.2 and 4.3, where each of them obey the equations (4.6). The flux field in which the particles are accelarated is obtained from the numerical solution of the model system (4.1) for different initial velocity profiles. The initial profiles for the density and the electric field are the same in both calculations and are given as dotted lines in figure 4.1.

Figure 4.2 corresponds to the small-amplitude approximation where ϵ is equal to $2 \cdot 10^{-3}$ (see appendix C). Besides, the initial distribution of the macro particles in phase space at $t = 0$, two further snapshots of the temporal evolution in phase space are seen. Due to the fact that the small-amplitude solution vary only a small amount in absolute scale (see figure 4.1), the phase space contour of the macro particle ensemble change its shape regular and smooth.
However, the situation changes dramatically since we consider the large-amplitude solution of (4.1), where ϵ is fixed to 0.2. This case can not treated analytically (see appendix C). The numerical results of our method are depicted in figure 4.3. The initial phase space coordinates of the macro particles are the same as already illustrated in the first picture of figure 4.2. As it is expected, the phase space contours which are shown in figure 4.3 for three different times reflect the distinct nonlinear behavior, inherent in the large-amplitude solution for systems like (4.1).
To complete the description of the figures 4.2 and 4.3, we have to explain the meaning of the drawn solid lines. In both figures these lines corresponds to the boundary curves

$$V_-(x,t) = \frac{1}{2}\left[2V_{ex}(x,t) - N_e(x,t)\right]$$

and

$$V_+(x,t) = \frac{1}{2}\left[2V_{ex}(x,t) + N_e(x,t)\right],$$

which are responsible for the temporal evolution of the distribution function $f_e(x, V_{ex}, t)$, necessary for the kinetic description of an incompressible thermal electron fluid as it is discussed in appendix C.

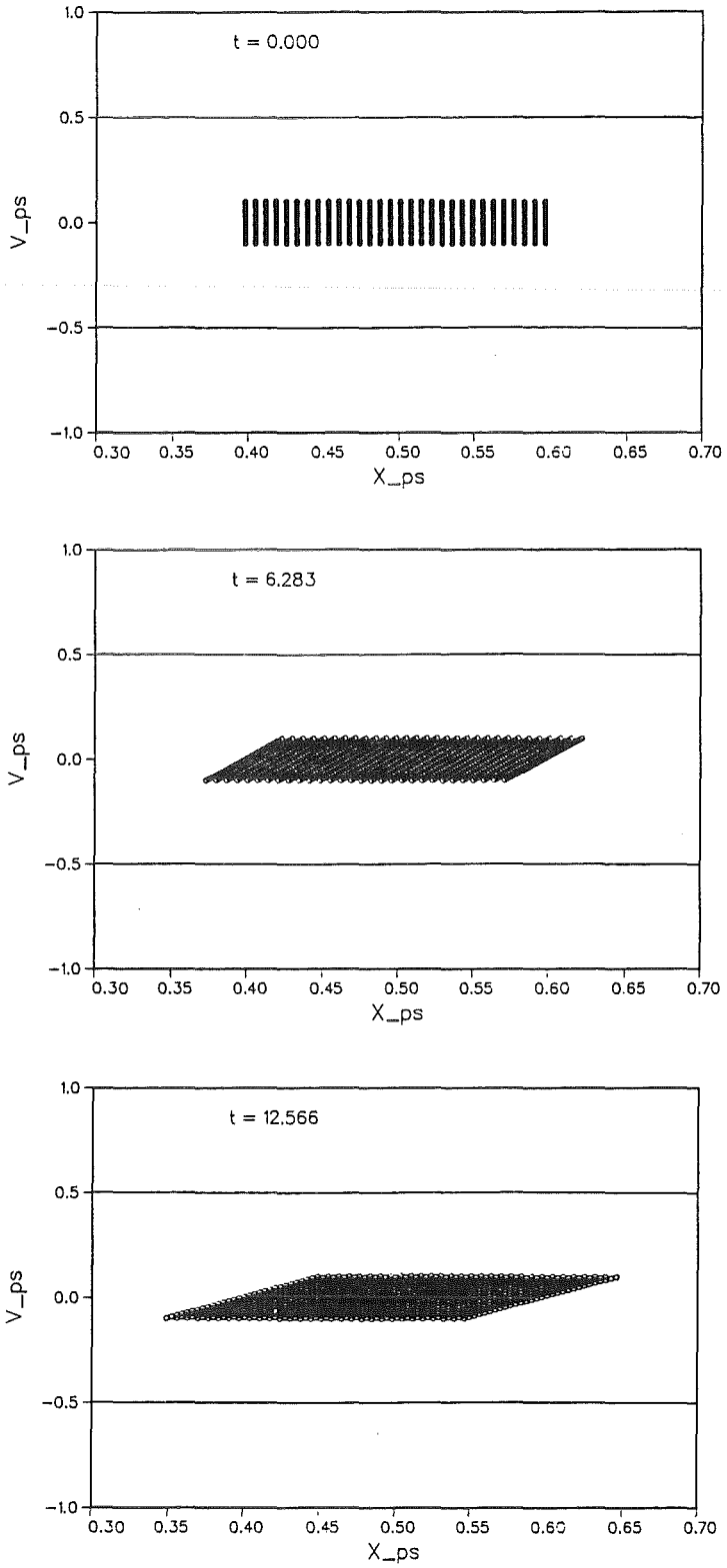

Figure 4.2: Phase space snapshots for different times of 900 macro particles, calculated in the small-amplitude approximation.

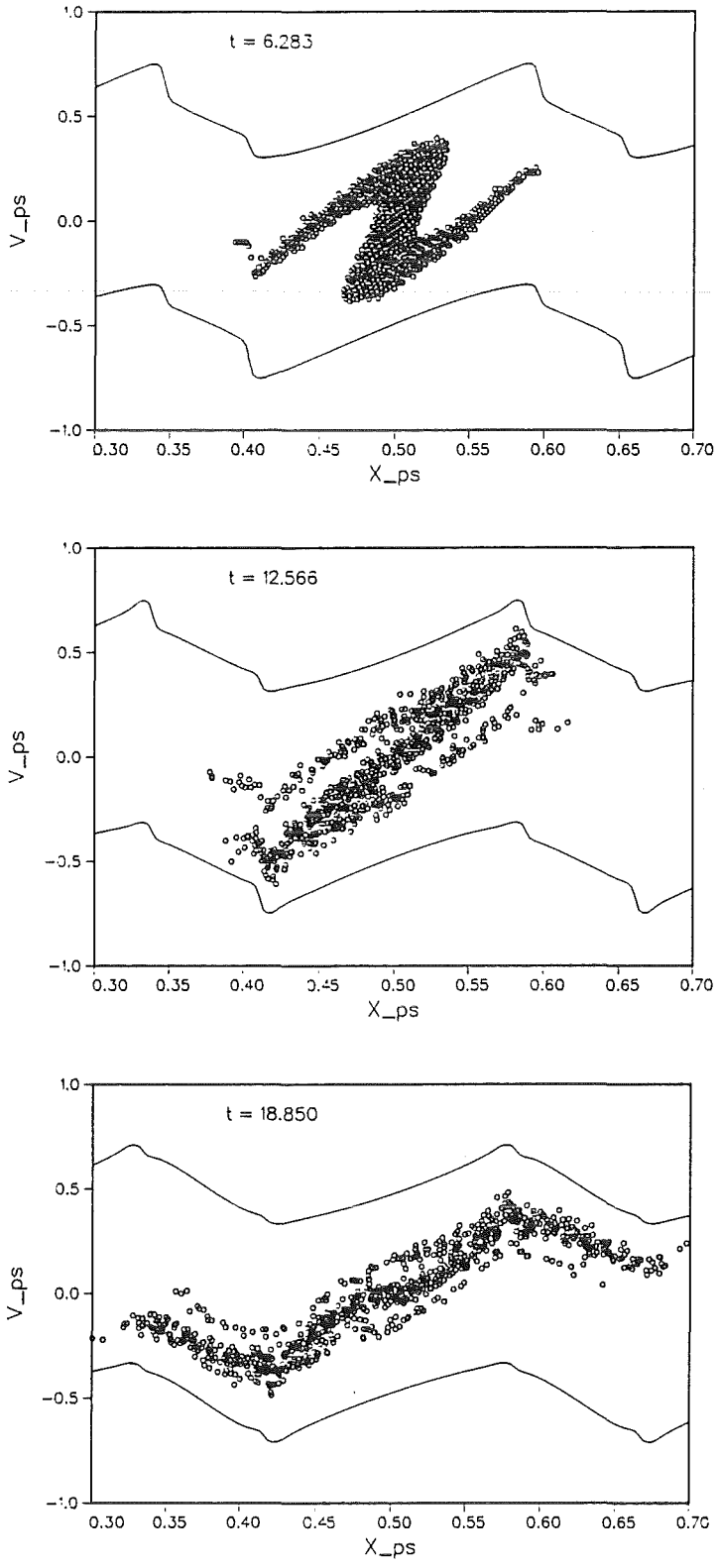

Figure 4.3: Phase space snapshots for different times of 900 macro particles, calculated in the large-amplitude limit.

B. Plasma expansion into vacuum

In this section we shall be concerned with the adiabatic expansion of a plasma into vacuum. Therefore, we have to solve the longitudinal model of a thermal two-component plasma (2.5), (2.6) with the numerical methods described in section III. The initial profiles of the conserved variables are initialized according (3.13), where $f = 3$ and x_0 is fixed equal to 50. The numerical calculations are performed on a grid with 200 equidistant grid zones covering a computational region from 0 to 200. The time step size Δt is controlled in an adaptive manner according the condition

$$\Delta t = \sigma \frac{\Delta x}{|a_{max}|},$$

where σ is hold fix to 0.4 and a_{max} is the maximum velocity of the propagating waves. Using the scheme in conservation form (3.3), the approximation of the flow within the plasma region is obtained from the HLL-method. A good estimation of the signal velocities a_l, a_r, necessary to determine the HLL-flux (3.4), should be given by the relations (4.2). To be consistent with the tracking algorithm (see III.C), which is in the form (3.14)-(3.16) accurate to the first order in space and time only, here we restrict ourselves to the original first order upwind scheme.

As a first test problem, we consider the homogeneous conservation laws (2.5) established by setting Ω_p equal to zero. Figure 4.4a shows the numerical result of the HLL-method combined with the tracking algorithm (3.14), (3.15) and the numerical flux calculation (3.17)-(3.19) near the plasma vacuum boundary. The results of the density, momentum, total energy and velocity are depicted for two different times. The numerical values are indicated by open squares ($t = 5$) and circles ($t = 10$), while the exact solution is plotted by a dashed ($t = 5$) and a solid ($t = 10$) line. Additionally, the dotted lines indicate the initial profiles of density and energy; for the momentum and velocity these lines coincide with the x-axis because they are zero. As it is represented by figure 4.4a, the agreement of the approximation with the exact solution is quite good. Since the numerical method applied is accurate to first order only, numerical dissipation is introduced resulting in a strong damping, which is clearly visible at the left boundary of the rarefaction fan.
This numerical damping is strongly reduced, if we use a second order extension of the HLL-scheme, as it is displayed in figure 4.4b. Here, we perform an additional slope calculation in the primitive variables (see e.g. [16]), which is switched off ten grid zones before the plasma vacuum boundary is reached.

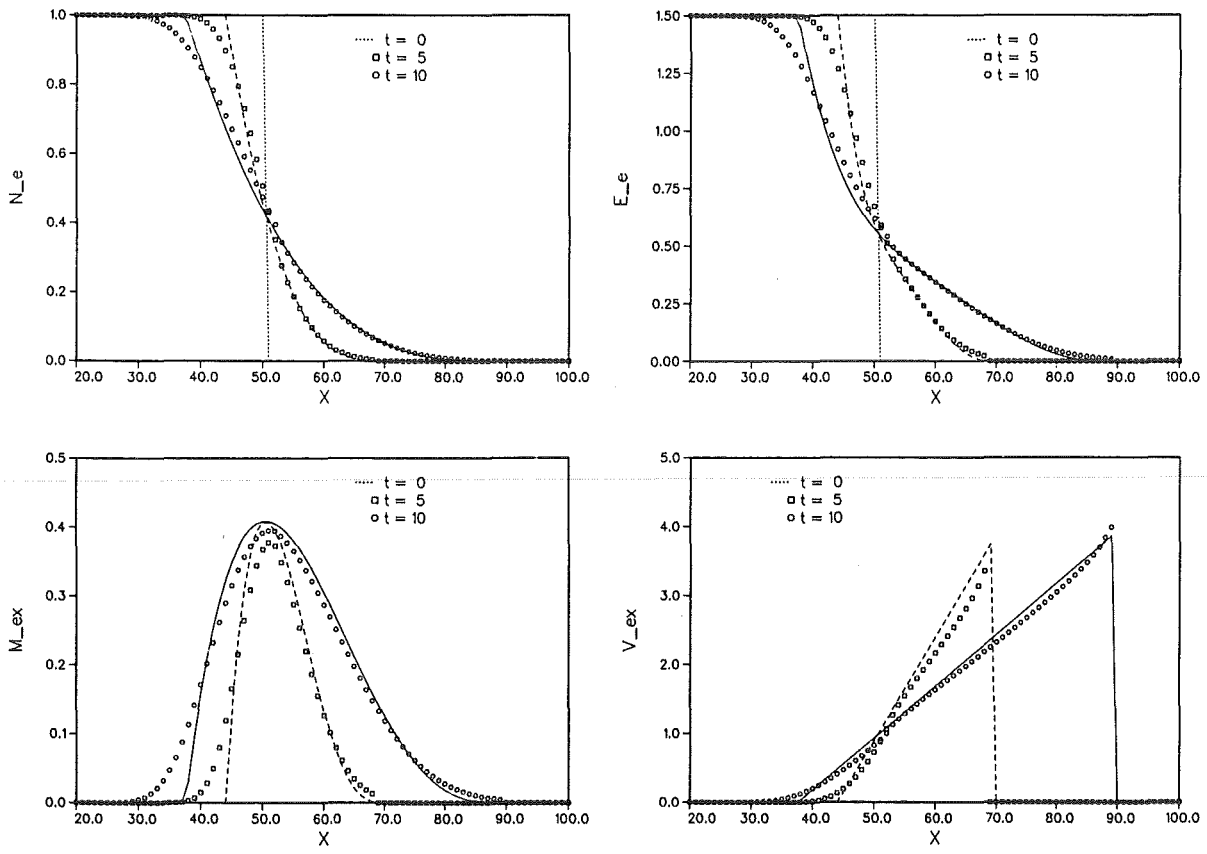

Figure 4.4a: Exact and numerical solution of the homogeneous conservation laws for different times, applying first order numerical methods.

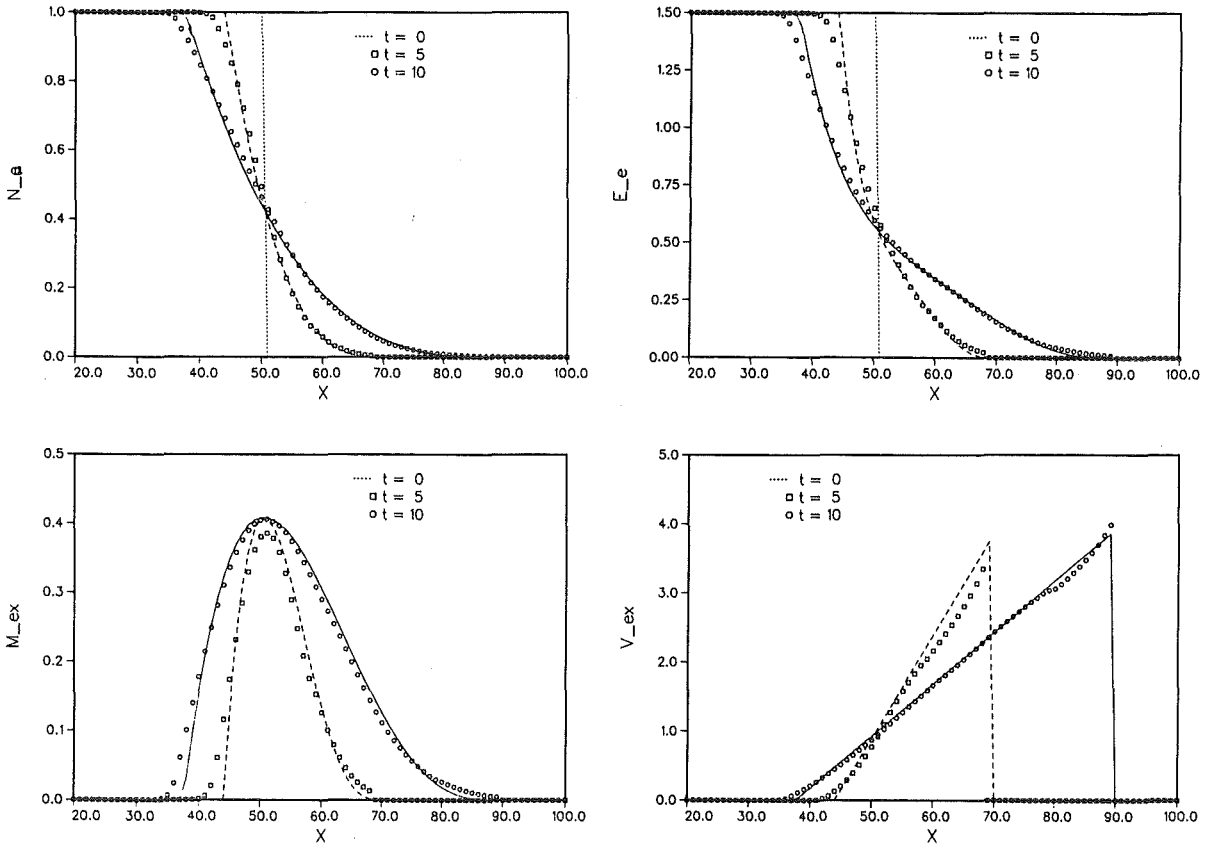

Figure 4.4b: Exact and numerical solution of the homogeneous conservation laws for different times, using a second order extension.

Munz remarked in [9] that the approximation of the location of the plasma vacuum boundary is much more sensitive than the approximation of the conservative variables. The reason for this is that the sound velocity of the left state is used for the evaluation of the propagation velocity V_v^n of the plasma vacuum boundary (see (3.14b)). Usually the sound velocity is calculated according the relation $C_{s\alpha} = \sqrt{\frac{\gamma \Pi_\alpha}{M_\alpha N_\alpha}}$, resulting in a much larger value of the sound velocity than the exact solution. This is due to the fact that in the vacuum limit the density and pressure as well as the quotient $\frac{\Pi_\alpha}{N_\alpha}$ tends to zero which is no longer valid in the numerical approximation. The quotient $\frac{\Pi_\alpha}{N_\alpha}$ near the vacuum is strongly influenced by the approximation errors, when Π_α and N_α tends to zero. A closer inspection of figure 4.4 shows that the numerical approximation of the total energy (and pressure, not shown here) slightly exceeds the line of the exact values near the vacuum transition, while those of the density are found to be on that line. Hence, the sound velocity does not tend to zero but to a finite value (in our problem to 0.7) and, consequently the propagation velocity V_v^n of the plasma vacuum boundary is larger than the exact one.
Considering the additional information that the waves expanding into vacuum are isentropic, we can approximate the full set of homogeneous conservation laws (2.5) by the corresponding isentropic equations. This means that the full set (2.5) reduces to two equations near the plasma vacuum boundary and the relation for the isentropic sound velocity becomes

$$C_{s\alpha} = \sqrt{\frac{\gamma}{M_\alpha} N_\alpha^{\gamma-1}}.$$

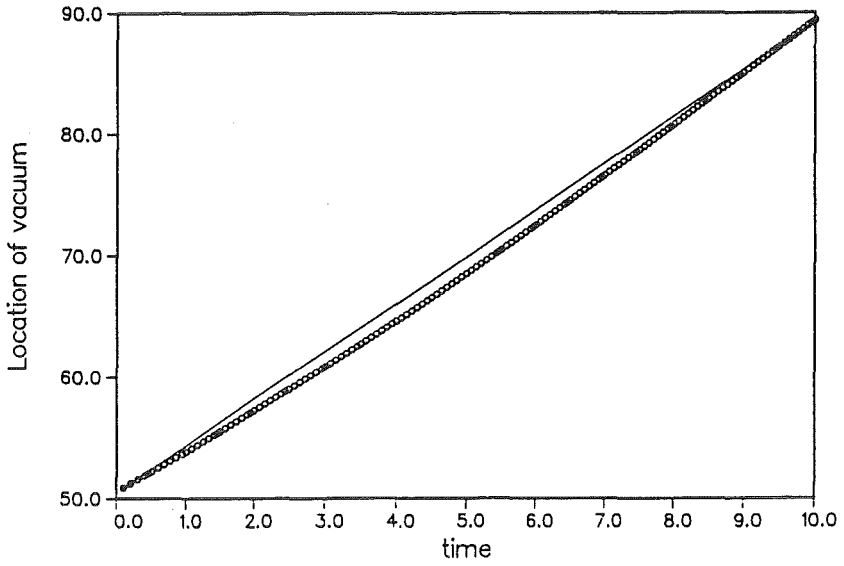

Figure 4.5: Location of plasma vacuum boundary as a function of time.

Using this relation for the determination of the sound velocity C_l and the calculation of the velocity V_v^n of the plasma vacuum boundary, the evaluation of the limit $\frac{\Pi_\alpha}{N_\alpha}$ can be circumvented, which results in a better approximation of the exact solution. The numerical result of the temporal evolution of the plasma vacuum boundary is displayed in figure 4.5 (open circles) in comparison with the exact solution (solid line). As it is seen, the use of the isentropic sound velocity leads to a slightly underestimation of the plasma vacuum location for a wide range in time. After approximately 9 time units the approximated plasma vacuum boundary come up with the exact one.

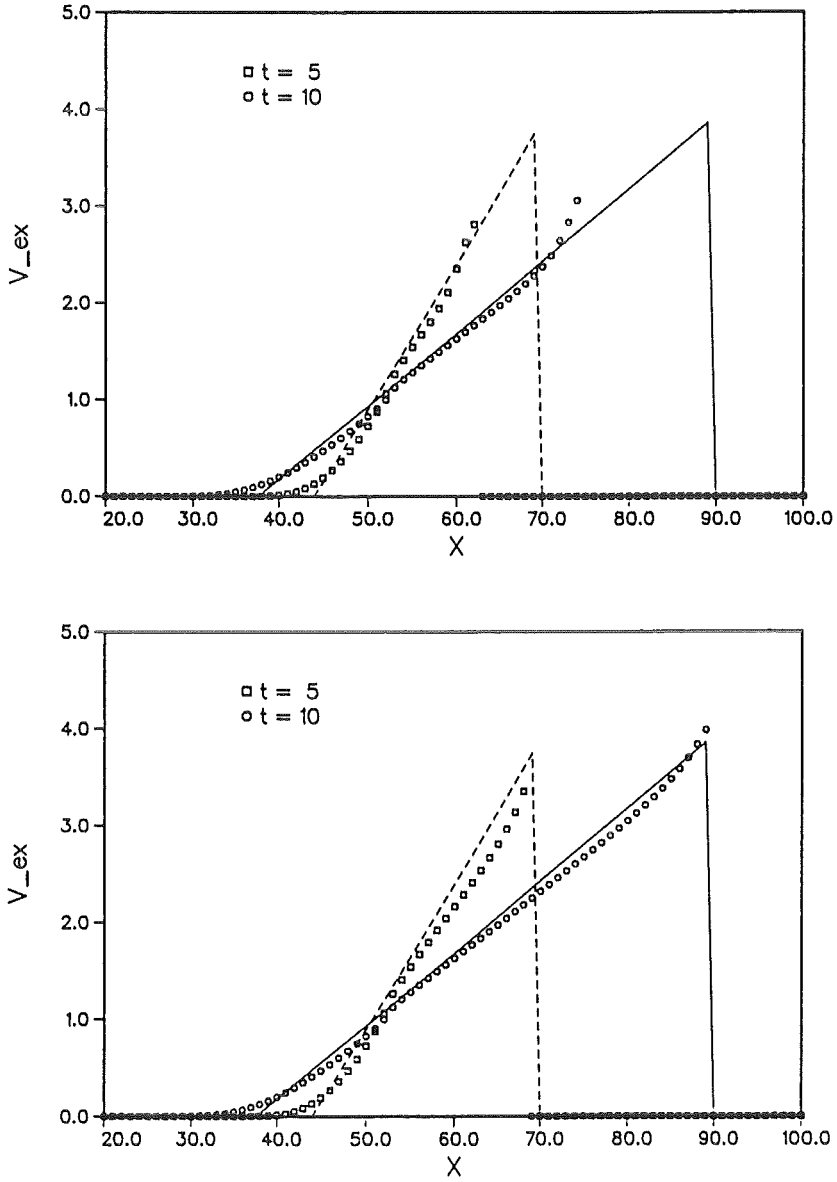

Figure 4.6: Influence of the calculation of the left state $\mathbf{u}_l$ of the VRP.

As well for the location (3.14) as for the flux calculation (3.19) at the plasma vacuum boundary it is necessary to have an appropriate approximation of the left state $\mathbf{u}_l$. To avoid that waves generated at $x_{i-1/2}$ do not reach the plasma vacuum interface, we introduce in III.C a constant left state according (3.15), where the right boundary of the interval length Δx coincide with the vacuum location X_v^n. As we already mention in III.C, it is favorable to evaluate the left state in the primitive variables according

$$\mathbf{u}_l = \alpha < \mathbf{w}_i^n > +(1-\alpha) \begin{pmatrix} N_{i-1}^n \\ V_{i-1}^n \\ \Pi_{i-1}^n \end{pmatrix},$$

where $< \mathbf{w}_i^n >$ is given by (3.16b). That this choice of the left state is a reasonable approximation is demonstrated once again in the second picture of figure 4.6, where the numerical result for the velocity (open squares and circles) is compared with the exact one (dashed and solid lines) for two different times. The same quantity is depicted in the first picture of figure 4.6 but for a different choice of the left state, namely

$$\mathbf{u}_l = \alpha < \mathbf{w}_i^n > .$$

It is obvious from figure 4.6 that this estimation of the left state leads to an insufficient approximation of the exact solutions, especially, in the vicinity of the plasma vacuum boundary.

The most interesting and challenging problem in this context is to consider the adiabatic expansion of two-component plasma (consisting of electrons and ions) into vacuum. Therefore, we have to solve numerically the inhomogeneous conservation laws (2.5a) for the electron and ion component of the plasma, respectively, which are coupled via the electric field, calculated from the Poisson equation (2.6). This should be the item of the second test problem, where all numerical techniques discussed in chapter III are required. Especially, the applicability of the explicit calculation of the electric field according (3.9) will be tested once again. Since the plasma expansion into vacuum should not be influenced by an external voltage, the time-dependent constant C^n is neglected.
Performing the numerical simulation the two components of the thermal plasma are initialized in the following manner. The initial profile of the negative charged ($Q_e = -1$) electron fluid with mass $M_e = 1$ is given by

$$\Big(N_e(x,0), \mathcal{M}_e(x,0), e_e(x,0)\Big) = \begin{cases} (1.0, 0.0, 1.5) & \text{for} \quad x < 50 \\ (0.0, 0.0, 0.0) & \text{for} \quad x > 50 \end{cases}$$

where we assume that $f = 3$ and the electron pressure $\Pi_e(x,0)$ is equal to one. The profiles of the positive charged ($Q_i = 1$) ion fluid with the mass $M_i = 100$ are

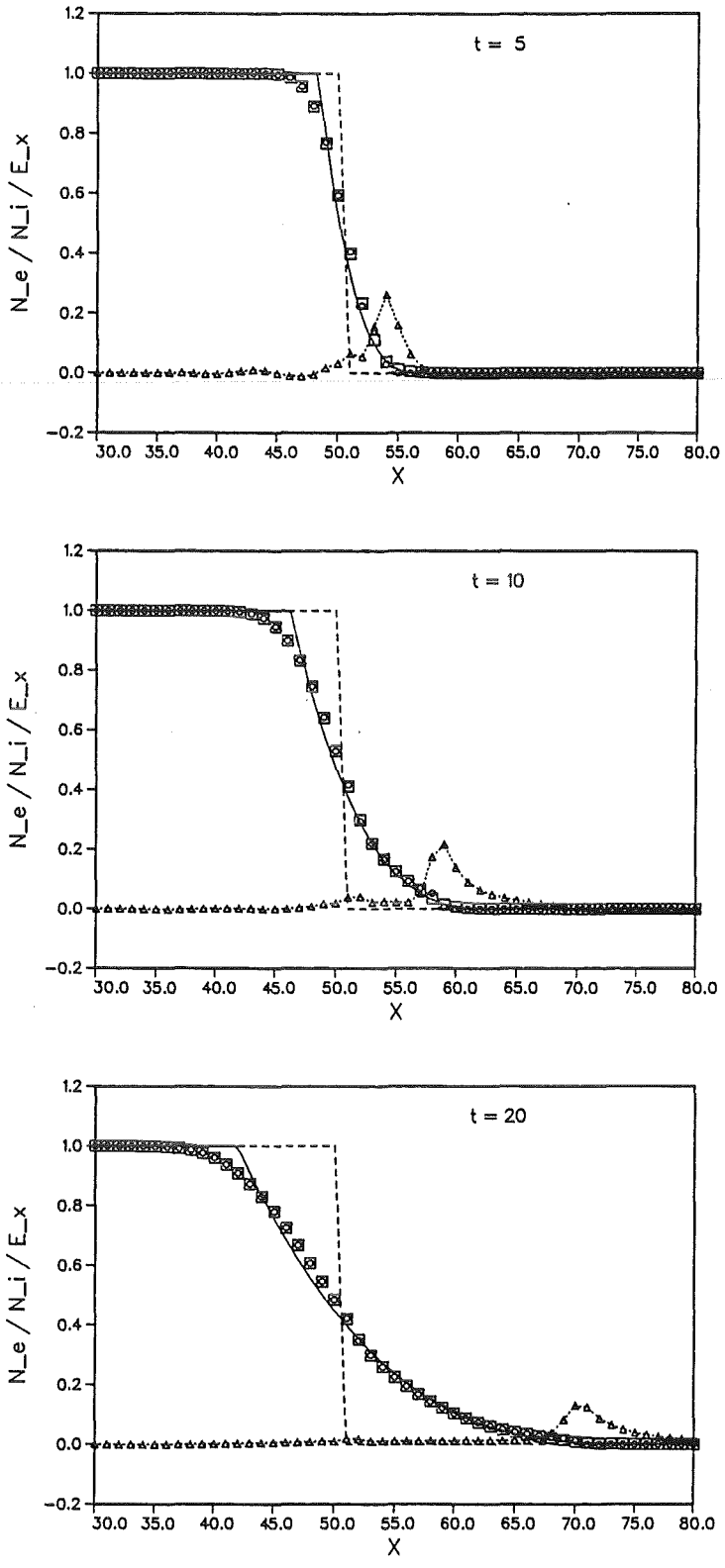

Figure 4.7: Temporal evolution of the electron (open squares) and ion (open circles) density solving the inhomogeneous conservation laws. The electric filed within the plasma is depicted as open triangles. Additionally, the exact single fluid solution (solid lines) is shown as a reference solution.

initialized according to

$$\Big(N_i(x,0), \mathcal{M}_i(x,0), e_i(x,0)\Big) = \begin{cases} (1.0, 0.0, 0.15) & \text{for} \quad x < 50 \\ (0.0, 0.0, 0.00) & \text{for} \quad x > 50 \end{cases}.$$

Here, we consider that the ion pressure is $\Pi_i(x,0) = 10$. Furthermore, for the first test calculations the dimensionless plasma frequency Ω_p, which plays the role of a coupling parameter for the plasma components, is choosen equal to 10.
Since the mass ratio between electrons and ions is small (0.01), we expect that the thermal two-component plasma considered behaves very similar as a single fluid plasma (obeying quasineutrality) expanding into vacuum. Hence, an appropriate reference solution should be obtained, if we solve the single fluid equations of a plasma according to appendix A. For that purpose, we have to fix the sound velocity (see A.2a) equal to

$$C = \sqrt{\frac{\gamma}{M_i}\Big(\Pi_e + \Pi_i\Big)} = 0.428,$$

to accommodate the initial values specified above.
In figure 4.7 the electron (open squares) and ion (open circles) density is depicted for three different times (corresponding to 63, 135, 285 circles in time), obtained from the numerical solution of thermal two-component plasma model (2.5), (2.6). Additionally, the dashed lines indicate the initial profiles of densitiy, while the solid lines represent the exact solution of the single fluid plasma model. We can ascertain from figure 4.7 that the calculated electron as well as the ion density are in good agreement with the exact single fluid density. A quantitative measure for the quasineutrality, observed in the most plasmas, may be the electric field within the plasma, which is plotted in figure 4.7 as open triangles connected by a dotted line. Besides, small wiggles occuring at early times, the electric field increases at the vicinity of the plasma vacuum interface. This reflects the fact that at the delicate numerical region (namely, the plasma vacuum boundary), the less mobility of the ions compared to the electrons plays an important role. We expect that, if we increase the coupling parameter Ω_p, the electric field tends to zero, resulting also in a more perfect quasineutral plasma at the plasma vacuum boundary. This will be the item of investigations, planned in the near future.

V. Summary and Outlook

As we have seen for three test problems, the high resolution upwind schemes combined with the tracking method and the proposed numerical flux calculation near the plasma vacuum boundary is an accurate and efficient tool to solve numerically the longitudinal model of a thermal two-component plasma. The numerical strategy applied is completed by using an explicit scheme to calculate the electric field which is a new approach in this context. The applicability of this approach is demonstrated with the aid of two examples. The results obtained are very encouraging and further investigations will be carried out to include an external voltage to get a more realistic model of the time-dependent behavior of ion diodes.

In near future, the one-dimensional time-dependent model will be extended to two space dimension. Solving this model numerically, we can refer to extensive experience made with the two-dimensional time-dependent hydrodynamic code HYDSOL [29] which use similar numerical methods as described in chapter III. In particular, it has been shown that the explicit second order Godunov-typ schemes could be vectorized in a very effective manner.

Appendix A:

Exact solution of the homogeneous conservation equations at a vacuum boundary

After some straightforward algebra, the homogeneous conservation equations - neglecting here the source term vector $\mathbf{q}(\mathbf{u}_\alpha)$ on the rhs of equation (2.5a) - can be written as

$$\frac{DN_\alpha}{Dt} = -N_\alpha \partial_x V_{\alpha x} \tag{A.1a}$$

$$\frac{DV_{\alpha x}}{Dt} = -\frac{1}{M_\alpha N_\alpha}\partial_x \Pi_\alpha \tag{A.1b}$$

$$\frac{D\Pi_\alpha}{Dt} + \gamma \Pi_\alpha \partial_x V_{\alpha x} = 0 \qquad \Leftrightarrow \qquad \frac{D}{Dt}\left(\frac{\Pi_\alpha}{N_\alpha^\gamma}\right) = 0 \tag{A.1c}$$

where the convective derivative is given by

$$\frac{D}{Dt} = \partial_t + V_{\alpha x}\partial_x. \tag{A.1d}$$

In the following we omit the index α, and put the velocity in x direction equal to $U = V_{\alpha x}$. Furthermore, we have to specify the initial data for which the equation (A.1) should be solved. Therefore, we suppose that there exist undisturbed values N_l, U_l and Π_l left from a point $x = x_0$. At the right side of this point, we imagine that there is vacuum. It is convenient at this stage to introduce the so-called self similar transformation

$$\xi = \frac{x - x_0}{C_l t} \tag{A.2a}$$

where C_l denotes the velocity of sound at the regime left from the point $x = x_0$. It is easy to show that the derivatives occuring in (A.1) can be expressed as

$$\partial_x = \frac{1}{C_l t}\partial_\xi \tag{A.2b}$$

$$\partial_t = -\frac{\xi}{t}\partial_\xi \tag{A.2c}$$

$$\frac{D}{Dt} = \frac{1}{t}\left(\frac{U}{C_l} - \xi\right)\partial_\xi \tag{A.2d}$$

where we make explicit use of the transformation (A.2a). From equation (A.1c) it is obvious that the scalar pressure is a function of the density only

$$\Pi(\xi) = \Pi_l \left(\frac{N(\xi)}{N_l}\right)^\gamma. \tag{A.3a}$$

According to equation (2.7d) the velocity of sound has the form

$$C(\xi) = C_l \left(\frac{N(\xi)}{N_l} \right)^{\frac{\gamma-1}{2}} \tag{A.3b}$$

where C_l is related to the initial values of pressure and density via

$$C_l = \sqrt{\frac{\gamma \Pi_l}{M N_l}}. \tag{A.3c}$$

Together with equations (A.2b), (A.2c) and (A.3a), we are left with a system of differential equations in ξ for the density $N(\xi)$ and the velocity $U(\xi)$. After a simple integration we obtain the following expression for the velocity

$$U(\xi) = \frac{\gamma - 1}{\gamma + 1} \left(V_{vac} + \frac{2C_l}{\gamma - 1} \xi \right) \tag{A.4a}$$

and for the density

$$N(\xi) = \left(\frac{\gamma - 1}{\gamma + 1} \right)^{\frac{2}{\gamma-1}} \frac{N_l}{C_l^{\frac{2}{\gamma-1}}} \left(V_{vac} - C_l \xi \right)^{\frac{2}{\gamma-1}} \tag{A.4b}$$

where the so-called vacuum velocity V_{vac} is given by

$$V_{vac} = U_l + \frac{2C_l}{\gamma - 1}. \tag{A.4c}$$

According the initial conditions for N_l, U_l and Π_l, it is obvious that the inequality

$$U_l - C_l \leq C_l \xi \leq U_l + \frac{2C_l}{\gamma - 1} \tag{A.4d}$$

define the range where the variable ξ holds.

Appendix B:

Analytical solution of the integrals occuring in (3.19)

We shall be concerned in this appendix with the analytical determination of the integrals occuring in (3.19). Changing the integration variable according the self-similar transformation

$$\xi = \frac{\delta y}{C_l t}, \tag{B.1a}$$

the integrals in (3.19) can be rewritten to the form

$$\mathrm{I}(\xi_1, \xi_2) = \frac{\delta y}{C_l} \int_{\xi_1}^{\xi_2} \frac{d\xi}{\xi^2} \mathbf{f}\left[\mathrm{u}(\xi)\right]. \tag{B.1b}$$

The boundaries of the integration are defined as

$$\xi_1 = \frac{\delta y}{C_l \delta t^*_{n+1}}, \qquad \xi_2 = \frac{\delta y}{C_l \delta t^*_n}. \tag{B.1c}$$

The vector of the fluxes

$$\mathbf{f} = \Big(f_1(\xi), f_2(\xi), f_3(\xi)\Big)^T$$

is obtained from the exact solution of the VRP. According appendix A the components of the flux vector are given by

$$\begin{aligned} f_1(\xi) &= N(\xi)U(\xi) \\ &= \alpha^{\nu+1} N_l C_l \Big(\xi_{max} - \xi\Big)^{\nu} \Big(\xi_{max} + \nu\xi\Big) \end{aligned} \tag{B.2a}$$

$$\begin{aligned} f_2(\xi) &= N(\xi)U^2(\xi) + \frac{1}{M}\Pi(\xi) \\ &= \alpha^{\nu+2} N_l C_l^2 \Big(\xi_{max} - \xi\Big)^{\nu} \Big(\xi_{max} + \nu\xi\Big)^2 \\ &\quad + \alpha^{\nu+2} \frac{\Pi_l}{M} \Big(\xi_{max} - \xi\Big)^{\nu+2} \end{aligned} \tag{B.2b}$$

$$\begin{aligned} f_3(\xi) &= \frac{1}{2} N(\xi)U^3(\xi) + \frac{f+2}{2} \frac{\Pi(\xi)}{M} U(\xi) \\ &= \frac{1}{2}\alpha^{\nu+3} N_l C_l^3 \Big(\xi_{max} - \xi\Big)^{\nu} \Big(\xi_{max} + \nu\xi\Big)^3 \\ &\quad + \frac{f+2}{2}\alpha^{\nu+3} \frac{\Pi_l}{M} C_l \Big(\xi_{max} - \xi\Big)^{\nu+2} \Big(\xi_{max} + \nu\xi\Big) \end{aligned}, \tag{B.2c}$$

where we use the abbreviation

$$\xi_{max} = \frac{V_{vac}}{C_l}$$

$$\nu = \frac{2}{\gamma - 1} \qquad (B.2d)$$

$$\alpha = \frac{\gamma - 1}{\gamma + 1}.$$

Obviously, the formal structure of the flux vector components f_i can be summarized in the following manner

$$\phi(\xi) = \Big(\xi_{max} - \xi\Big)^{\sigma}\Big(\xi_{max} + \nu\xi\Big)^{\mu}.$$

Therefore, we only have to evaluate the integral

$$J(\xi_1, \xi_2) = \int_{\xi_1}^{\xi_2} d\xi \frac{1}{\xi^2}\Big(\xi_{max} - \xi\Big)^{\sigma}\Big(\xi_{max} + \nu\xi\Big)^{\mu}, \qquad (B.3a)$$

which can be done in an elementary way if the exponents $\sigma, \mu \in \mathcal{N}_0$. This is surely true, if we consider a perfect gas, where ν can take the values $\nu = \{1, 2, 3, 5, 6\}$. Expanding the factors in (B.3a) into binominal power series and performing several rearrangements, we are left with the expression

$$J(\xi_1, \xi_2) = \sum_{k=0}^{\sigma}\sum_{m=k}^{\mu+k}(-1)^k \nu^{m-k}\binom{\sigma}{k}\binom{\mu}{m-k}\xi_{max}^{\sigma+\mu-m}\int_{\xi_1}^{\xi_2} d\xi\xi^{m-2}, \qquad (B.3b)$$

where $\binom{m}{n}$ denotes the usual binominal coefficient. Splitting up the summation occuring in (B.3b) and performing the integration, we finally obtain the longish, but very simple result for the exact integration of (B.3a)

$$\begin{aligned} J(\xi_1, \xi_2) = {} & \xi_{max}^{\sigma+\mu}\left(\frac{1}{\xi_1} - \frac{1}{\xi_2}\right) \\ & + \xi_{max}^{\sigma+\mu-1}\Big(\nu\mu - \sigma\Big)\ln\left(\frac{\xi_2}{\xi_1}\right) \\ & - \xi_{max}^{\sigma-1}\frac{\nu^{\mu}\sigma}{\mu}\Big(\xi_2^{\mu} - \xi_1^{\mu}\Big) \\ & + \sum_{m=2}^{\mu}\xi_{max}^{\sigma+\mu-m}\frac{\nu^{m-1}}{m-1}\binom{\mu}{m-1}\left[\frac{\nu}{m}(\mu - m + 1) - \sigma\right]\Big(\xi_2^{m-1} - \xi_1^{m-1}\Big) \\ & + \sum_{k=2}^{\sigma}\sum_{m=k}^{\mu+k}\xi_{max}^{\sigma+\mu-2}\frac{(-1)^k\nu^{m-k}}{m-1}\binom{\sigma}{k}\binom{\mu}{m-k}\Big(\xi_2^{m-1} - \xi_1^{m-1}\Big). \end{aligned} \qquad (B.3c)$$

Appendix C:

The finite electron pressure model

Rewriting the inhomogeneous conservation laws (2.5a) in a form convenient for the following considerations we are left with

$$\frac{DN_\alpha}{Dt} = -N_\alpha \partial_x V_{\alpha x} \qquad (C.1a)$$

$$\frac{DV_{\alpha x}}{Dt} = -\frac{1}{M_\alpha N_\alpha}\partial_x \Pi_\alpha + S_\alpha E_x \qquad (C.1b)$$

$$\frac{D}{Dt}\left(\frac{\Pi_\alpha}{N_\alpha^3}\right) = 0 \qquad \Leftrightarrow \qquad \Pi_\alpha = N_\alpha^3 \qquad (C.1c)$$

$$\partial_x E_x = \sum_\alpha S_\alpha M_\alpha N_\alpha \qquad (C.1d)$$

where the convective derivative is given by equation (A.1d). Furthermore, we assume that the $\gamma = 3$ adiabatic pressure law (C.1c) holds which means that the degree of freedom of the perfect gas is $f = 1$.
A special class of models in plasma physics assume, that the ions form a fixed, uniform background (see e.g. [27]). In other words this means that, if the ion mass M_i goes to infinity, the ion pressure ($\frac{\Pi_i}{M_i} \to 0$) as well as the electric field ($\frac{E_x}{M_i} \to 0$) in the ion equation can be neglected. With the additional assumption that the density and velocity is equal to one and zero, respectively, the system (C.1) for the ions has a simple form

$$N_i(x,t) = 1$$

$$V_{ix}(x,t) = 0, \qquad (C.2)$$

which holds for all times. The resulting motion of the electron fluid is finally obtained from the model equations

$$\frac{DN_e}{Dt} = -N_e \partial_x V_{ex} \qquad (C.3a)$$

$$\frac{DV_{ex}}{Dt} = -\frac{1}{N_e}\partial_x \Pi_e + \Omega_p E_x \qquad (C.3b)$$

$$\frac{DE_x}{Dt} = \Omega_p V_{ex} \qquad (C.3c)$$

$$\Pi_e = N_e^3, \qquad (C.3d)$$

where $\Omega_p = \omega_{p0} t_0$ denotes the dimensionsless plasma frequency. Furthermore, we take into account that the dimensionless electron charge $Q_e = -1$ and the mass of the electrons $M_e = 1$. Introducing the transformation into Lagrangean coordinates as

$$\tau = t$$

$$\zeta = x - \int_0^\tau dT V_{ex}(\zeta, T), \tag{C.4}$$

the model equations of the thermal electron fluid (C.3) can be written in the following form (see e.g. [27])

$$N_e(\zeta, \tau) = \frac{1}{1 + \int_0^\tau dT \partial_\zeta V_{ex}(\zeta, T)} \tag{C.5a}$$

$$\Pi_e(\zeta, \tau) = N_e^3(\zeta, \tau) \tag{C.5b}$$

$$\partial_\zeta E_x(\zeta, \tau) = \Omega_p V_{ex}(\zeta, \tau) \tag{C.5c}$$

$$\partial_\zeta^2 V_{ex}(\zeta, \tau) + \Omega_p^2 V_{ex}(\zeta, \tau) = 3\partial_\zeta \left\{ \frac{\partial_\zeta V_{ex}(\zeta, \tau)}{\left[1 + \int_0^\tau dT \partial_\zeta V_{ex}(\zeta, \tau)\right]^4} \right\} \tag{C.5d}$$

where we assumed that the initial density profile of the electrons satisfy the condition

$$N_e(\zeta, 0) = 1. \tag{C.5e}$$

Obviously, equation (C.5d) is not tractable analytically without some additional approximations. In the small-amplitude analysis, the linearized version of (C.5d) is given by

$$\partial_\tau^2 V_{ex}^{(1)}(\zeta, \tau) + \Omega_p^2 V_{ex}^{(1)}(\zeta, \tau) = 3\partial_\zeta^2 V_{ex}^{(1)}(\zeta, \tau) \tag{C.6a}$$

where we put $V_{ex}(\zeta, \tau)$ equal to

$$V_{ex}(\zeta, \tau) = \epsilon V_{ex}^{(1)}(\zeta, \tau), \qquad 0 < \epsilon \ll 1. \tag{C.6b}$$

Assuming that the initial acceleration of the electron fluid is equal zero

$$\partial_\tau V_{ex}(\zeta, \tau)|_{\tau=0} = 0, \tag{C.7a}$$

and interested within this context in nonlinear periodic solutions of (C.5) with the initial condition

$$V_{ex}^{(1)}(\zeta, \tau) = \sin \zeta, \tag{C.7b}$$

we finally obtain the solution of the approximated model system:

$$V_{ex}(\zeta,\tau) = \epsilon \sin\zeta \cos\beta\tau \tag{C.8a}$$

$$E_x(\zeta,\tau) = \frac{\epsilon\Omega_p}{\beta} \sin\zeta \sin\beta\tau \tag{C.8b}$$

$$N_e(\zeta,\tau) = \frac{1}{1+\frac{\epsilon}{\beta}\cos\zeta\sin\beta\tau} \tag{C.8c}$$

$$\Pi_e(\zeta,\tau) = N_e^3(\zeta,\tau), \tag{C.8d}$$

where the modified frequency β is given by the expression

$$\beta = \sqrt{\Omega_p^2 + 3}. \tag{C.8e}$$

The physical importance of the thermal electron model (C.3) arise from the fact, that the macroscopic equations (C.3) are equivalent to the single-water-bag model in the kinetic description of the electron fluid (see [27] and references therein). To recognize the close relation between the microscopic and macroscopic describtion, we suppose that the initial distribution function of the electrons $f_e(x,V,t)$ ($V = V_{ex}$) is given by (see figure C.1)

$$f_e(x,V,0) = \begin{cases} A = const. > 0, & V_-(x,0) < V < V_+(x,0) \\ 0 \qquad otherwise \end{cases}.$$

The temporal evolution of f_e is given by the Vlasov-Maxwell equation, which reads as

$$\partial_t f_e + V\partial_x f_e - \Omega_p E_x \partial_V f_e = 0 \tag{C.9a}$$

$$\partial_x E_x = \Omega_p\Big(1 - N_e\Big), \tag{C.9b}$$

describing the incompressible motion of the electron fluid in phase space. Furthermore, we suppose that the boundary curves V_- and V_+ evolves temporally in such a manner that at time t the distribution function is given by

$$f_e(x,V,t) = \begin{cases} A = const. > 0, & V_-(x,t) < V < V_+(x,t) \\ 0 \qquad otherwise \end{cases}. \tag{C.10}$$

As a consequence of taking the appropriate moments of the Vlasov equation (C.9a), the boundary curves $V_-(x,t)$ and $V_+(x,t)$ are related to the density, velocity and pressure. Assuming that $V_-(x,t)$ and $V_+(x,t)$ are single-valued functions of x, we find that the local densities of interest can be expressed as

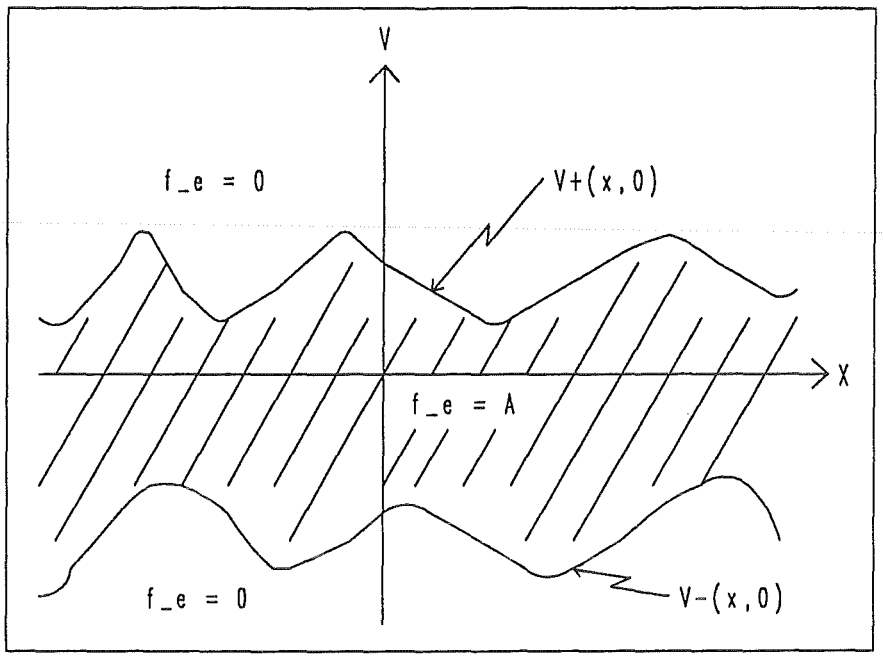

Figure C.1: Phase space of the electrons at t=0.

$$N_e(x,t) = \int_{-\infty}^{\infty} dV f_e(x,V,t) = A\left(V_+(x,t) - V_-(x,t)\right) \qquad (C.11a)$$

$$V_{ex}(x,t) = \frac{1}{N_e(x,t)} \int_{-\infty}^{\infty} dV V f_e(x,V,t) = \frac{1}{2}\left(V_+(x,t) + V_-(x,t)\right) \qquad (C.11b)$$

$$\Pi_e(x,t) = M_e \int_{-\infty}^{\infty} dV \left[V - V_{ex}(x,t)\right]^2 f_e(x,V,t) = \frac{M_e}{12} A \left(V_+(x,t) - V_-(x,t)\right)^3. \qquad (C.11c)$$

However, the heat flux of the electrons, defined as

$$h_{ex}(x,t) = \frac{M_e}{2} \int_{-\infty}^{\infty} dV \left[V - V_{ex}(x,t)\right]^3 f_e(x,V,t),$$

is identically zero.

References

1. V.M. Bystritskii and A.N. Didenko; High-Power Ion Beams, AIP Translation Series, New York, 1989.

2. H. Bluhm, K. Böhnel, L. Buth, P. Hoppé, H.U. Karow, A. Klumpp, D. Rusch, T. Scherer, U. Schülken and J. Singer; in Digest of Technical Papers, 5th IEEE Pulsed Power Conf., Arlington, 1985, p.114.

3. K.W. Zieher and O. Stoltz; Proc 4th Int. Topical Conf. on High-Power Electron and Ion-Beam Research and Technology, Paliseau (France), 1981. Eds. H.J. Doucet and J.M Buzzi, p.379.
   K.W. Zieher; Nucl. Instr. Meth. **228**, 161 (1984).

4. W. Schimassek; **KfK 4554**, Karlsruhe, 1989.
   W. Schimassek, W. Bauer and O. Stoltz; Rev. Sci. Instrum. **62**, 168 (1991).

5. H. Bluhm, P. Hoppé, H. Bachmann, W. Bauer, K. Baumung, L. Buth, H.U. Karow, H. Laqua, D. Rusch, E. Stein and O. Stoltz; IEEE Trans. Plasma Sci., in press.

6. T. Westermann; **KfK 4510**, Karlsruhe, 1989.
   T. Westermann; Nucl. Instr. Meth. A **281**, 253 (1989).
   T. Westermann; Nucl. Instr. Meth. A **290**, 529 (1990).

7. C.K. Birdsall and A.B. Langdon; Plasma Physics via Computer Simulation, McGraw-Hill, New York, 1985.

8. T. Westermann; Appl. Phys. Lett. **58**, 696 (1991).

9. C.-D. Munz; A tracking method for gas flow into vacuum based on vacuum Riemann problem, to appear in Math. Meth. in Appl. Science.

10. R. Balescu; Transport Processes in Plasmas, North-Holland, Amsterdam, 1988.

11. D.R. Nicholson; Introduction to Plasma Theory, Wiley Sons, New York, 1983.

12. J.P. Freidberg; Ideal Magnetohydrodynamics, Plenum Press, New York 1987.

13. K.H. Spatschek; Theoretische Plasmaphysik, Teubner, Stuttgart, 1990.

14. S.J Braginskii; Transport Processes in a Plasma, in: Reviews of Plasma Physic, Vol. 1, Consultans Bureau, New York, 1965. (ed. M.A. Leontovich).

15. R. Schneider and C.-D. Munz; Modellierung des kalten Plasmas mit Hilfe zeitabhängiger magnetohydrodynamischer Methoden, **KfK 5053**, Karlsruhe,

1992.
R. Schneider; Two-Fluid Plasma Simulations with Explicit Numerical Methods, Proc. of the Joint Int. Conf. on Mathematical Methods and Supercomputing in Nuclear Applications, Karlsruhe, 1993. Eds. H. Küsters, E. Stein, W. Werner, p. 71.

16. R.J. LeVeque; Numerical Methods for Conservation Laws, Birkhäuser, Basel, 1990.
17. S.K. Godunov; Mat. Sbornik **47**, 271(1959).
18. A. Harten, P.D. Lax and B. van Leer; SIAM Rev. **25**, 35 (1983).
19. C.-D. Munz; Godunov-Typ Verfahren für die Gleichungen der kompressiblen Strömungsmechanik, **KfK 5058**, Karlsruhe, 1992.
20. B. van Leer; J. Comput. Phys. **32**, 101(1979).
21. G.I. Marchuk; Methods of Numerical Mathematics, Springer-Verlag, New York / Heidelberg / Berlin, 1975.
22. G. Engeln-Müllges and F. Reuter; Fortransammlung zur Numerischen Mathematik mit Standard FORTRAN 77 - Programmen, B.I., Mannheim, 1988.
23. W. Hackbusch; Elliptic Differential Equations, Springer- Verlag, Berlin / Heidelberg, 1992.
24. W.H. Press, B.P. Flannery, S.A. Teukosky and W.T. Vetterling; Numerical Receipes, Cambridge University Press, Cambridge, 1987.
25. A. Kadish, W. Peter and M.E Jones; Appl. Phys. Lett. **47**, 115 (1985).
26. E. Halter; Math. Meth. in Appl. Sci. **7**, 101 (1985).
27. R.C. Davidson, Methods in Nonlinear Plasma Theory, Academic Press, New York, 1972.
28. P.L. Roe; J. Compt. Phys. **43**, 357 (1982).
29. C.-D. Munz and S. Hirmer; Karlsruhe 1992, unpublished.